1983

Elastic behavior of single crystals of ytrria-stabilized zirconia

Hamdi M. Kandil
Iowa State University

INFORMATION TO USERS

This reproduction was made from a copy of a document sent to us for microfilming. While the most advanced technology has been used to photograph and reproduce this document, the quality of the reproduction is heavily dependent upon the quality of the material submitted.

The following explanation of techniques is provided to help clarify markings or notations which may appear on this reproduction.

1. The sign or "target" for pages apparently lacking from the document photographed is "Missing Page(s)". If it was possible to obtain the missing page(s) or section, they are spliced into the film along with adjacent pages. This may have necessitated cutting through an image and duplicating adjacent pages to assure complete continuity.

2. When an image on the film is obliterated with a round black mark, it is an indication of either blurred copy because of movement during exposure, duplicate copy, or copyrighted materials that should not have been filmed. For blurred pages, a good image of the page can be found in the adjacent frame. If copyrighted materials were deleted, a target note will appear listing the pages in the adjacent frame.

3. When a map, drawing or chart, etc., is part of the material being photographed, a definite method of "sectioning" the material has been followed. It is customary to begin filming at the upper left hand corner of a large sheet and to continue from left to right in equal sections with small overlaps. If necessary, sectioning is continued again–beginning below the first row and continuing on until complete.

4. For illustrations that cannot be satisfactorily reproduced by xerographic means, photographic prints can be purchased at additional cost and inserted into your xerographic copy. These prints are available upon request from the Dissertations Customer Services Department.

5. Some pages in any document may have indistinct print. In all cases the best available copy has been filmed.

University Microfilms International
300 N. Zeeb Road
Ann Arbor, MI 48106

Kandil, Hamdi M.

ELASTIC BEHAVIOR OF SINGLE CRYSTALS OF YTRRIA-STABILIZED ZIRCONIA

Iowa State University PH.D. 1983

Elastic behavior of single crystals of ytrria-stabilized zirconia

by

Hamdi M. Kandil

A Dissertation Submitted to the
Graduate Faculty in Partial Fulfillment of the
Requirements for the Degree of
DOCTOR OF PHILOSOPHY

Department: Materials Science and Engineering
Major: Metallurgy

Approved:

Signature was redacted for privacy.

In Charge of Major Work

Signature was redacted for privacy.

For the Major Department

Signature was redacted for privacy.

For the Graduate College

Iowa State University
Ames, Iowa

1983

TABLE OF CONTENTS

		Page
1.	INTRODUCTION	1
	1.1. Structural Considerations in ZrO_2-Y_2O_3 System	1
	1.2. Phase Relationships in ZrO_2-Y_2O_3 System	7
	1.3. Elasticity and Wave Propagations in Crystals	12
	1.4. Single Crystal Elastic Constants of YSZ	14
2.	EXPERIMENTAL PROCEDURES	15
	2.1. Sample Preparation and Characterization	15
	2.2. Ultrasonic Measurements	18
3.	RESULTS AND DISCUSSION	24
4.	SUMMARY	57
5.	BIBLIOGRAPHY	60
6.	APPENDIX	64
7.	ACKNOWLEDGEMENTS	73

LIST OF TABLES

		Page
Table 1.	Summary of wave mode-elastic constant relations in cubic crystals	13
Table 2.	Compositions and dimensions of YSZ crystals	17
Table 3.	Lattice constants and densities of YSZ crystals	19
Table 4.	Comparison of room temperature elastic constants for YSZ crystals with literature data	25
Table 5.	Debye temperatures of YSZ crystals at room temperature	31
Table 6.	Variations of longitudinal and shear constants along different directions in YSZ crystals at room temperature	47
Table 7.	Variation of Cauchy relation with temperature for YSZ crystals	50
Table 8.	Internal consistency of redundant evaluation at room temperature	52
Table 9.	Variation of single-crystal elastic constants with temperature of 11.1 m/o YSZ before and after thermal expansion correction	65
Table 10.	Variation of single-crystal elastic constants with temperature of 12.1 m/o YSZ before and after thermal expansion correction	66
Table 11.	Variation of single-crystal elastic constants with temperature of 15.5 m/o YSZ before and after thermal expansion correction	67

Page

Table 12. Variation of single-crystal elastic constants with temperature of 17.9 m/o YSZ before and after thermal expansion correction 68

Table 13. Polycrystalline moduli of 11.1 m/o YSZ at different temperatures 69

Table 14. Polycrystalline moduli of 12.1 m/o YSZ at different temperatures 70

Table 15. Polycrystalline moduli of 15.5 m/o YSZ at different temperatures 71

Table 16. Polycrystalline moduli of 17.9 m/o YSZ at different temperatures 72

LIST OF FIGURES

		Page
Figure 1.	Ideal fluorite structure in YSZ	2
Figure 2.	Oxygen coordination polyhedra; (a) idealized MO_7 group characteristic of ZrO_2 and (b) basic fluorite MO_8 group	4
Figure 3.	The C-type rare earth oxide structure and the six-fold coordination in Y_2O_3	6
Figure 4.	ZrO_2-Y_2O_3 phase diagram according to Scott [11]	9
Figure 5.	ZrO_2-Y_2O_3 phase diagram according to Pascual and Duran [12]	10
Figure 6.	Block diagram of the ultrasonic pulse-echo-overlap apparatus	20
Figure 7.	Experimental arrangement for ultrasonic wave velocity measurements above room temperature	23
Figure 8.	Compositional dependencies of C_{11}, C_{12}, and C_{44} for YSZ crystals at room temperature. The solid symbols are used to differentiate the 8.1 m/o Y_2O_3 crystal from the others because the temperature dependencies of the elastic constants for this crystal were not reproducible, although the room temperature constants were reproducible	26
Figure 9.	Variation of Debye temperatures of YSZ crystals with the square root of the inverse mass per formula at room temperature	32
Figure 10.	Temperature dependence of the longitudinal wave velocity $V_{L[110]}$ for the 8.1 m/o Y_2O_3 crystal, measured at different times; (1) initial measurement, (b) after 5 days, (c) after 2 weeks, (d) after 5 weeks, and (e) after 10 weeks	34

Page

Figure 11. Temperature dependence of the fast shear wave velocity $V_{VT1[1\bar{1}0]}$ for the 8.1 m/o Y_2O_3 crystal. Runs 1 and 2 were measured 10 weeks apart 36

Figure 12. Temperature dependence of the slow shear wave velocity $V_{VT2[001]}$ for the 8.1 m/o Y_2O_3 crystal. Runs 1 and 2 were measured 10 weeks apart 37

Figure 13. Temperature dependence of C_{11} for YSZ crystals 38

Figure 14. Temperature dependence of C_{12} for YSZ crystals 39

Figure 15. Temperature dependence of C_{44} for YSZ crystals 40

Figure 16. Temperature dependence of C' for YSZ crystals 41

Figure 17. Temperature dependence of C_L for YSZ crystals 42

Figure 18. Variation of shear anisotropy with composition of YSZ crystals at different temperatures. The 8.1 m/o Y_2O_3 value is shown in a different symbol (x) for the same reason as before 45

Figure 19. Variations of longitudinal and shear constants along different directions in YSZ crystals at room temperature. The 8.1 m/o Y_2O_3 values are shown in solid symbols for the same reason as before 48

Figure 20. Variations of polycrystalline moduli with composition of YSZ at room temperature. The 8.1 m/o Y_2O_3 values are shown in solid symbols for the same reason as before 54

Page

Figure 21. Comparison of the temperature dependence of the relative Young's modulus of the 17.9 m/o YSZ and 20 m/o YSH. The relative modulus is defined as the ratio of the modulus at a specific temperature to the modulus at room temperature 56

1. INTRODUCTION

There is growing interest in stabilized zirconia (zirconium dioxide, ZrO_2) in both scientific and technical fields. It is used as a solid electrolyte to determine thermodynamic quantities from oxide potential measurements, and it is used in the investigation of kinetic phenomena, such as the mobility of oxygen in metals or chemical diffusion in metal oxides. In practical applications, an yttria-stabilized zirconia[1]-solid electrolyte can serve in a device to measure and adjust the oxygen content in gases, as an oxygen monitor during reduction of ores, and as a membrane in high temperature fuel cells [1]. YSZ is also used for artistic purposes as artificial diamond.

1.1. Structural Considerations in ZrO_2-Y_2O_3 System

Pure zirconia is polymorphic with the following transformations [2]:

monoclinic $\underset{\sim}{1170°C}$ tetragonal $\underset{\sim}{2370°C}$ cubic $\underset{\sim}{2680°C}$ liquid.

Both monoclinic and tetragonal forms are slightly distorted forms of the fluorite structure (Fig. 1). The monoclinic structure of ZrO_2 is characterized by the spatial arrange-

---

[1]In this thesis, yttria-stabilized zirconia will be written YSZ.

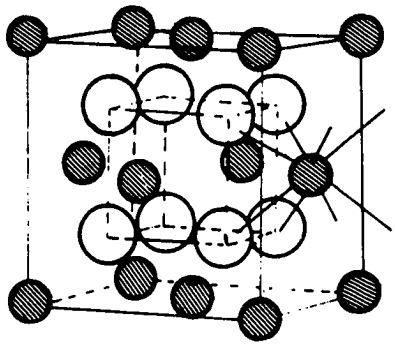

● Zr or Y : (0,0,0), (1/2,1/2,0), (1/2,0,1/2), and (0,1/2,1/2)

○ O : (1/4,1/4,1/4), (3/4,3/4,1/4), (3/4,1/4,3/4), (1/4,3/4,3/4), (3/4,3/4,3/4), (5/4,5/4,3/4), (5/4,3/4,5/4), and (3/4,5/4,5/4)

Figure 1. Ideal fluorite structure in YSZ

ment of ZrO_2 coordination polyhedra [3]. The coordination polyhedron has been visualized as being derived from a cube. Four of the oxygen atoms are at each corner of the base of a cube in a planar array and one at one of the upper corners. The remaining two oxygens are at the midpoints of the cube edges connecting the unoccupied corners. The resulting polyhedron very closely resembles the basic MO_8 coordination group used in describing the fluorite structure (Fig. 2).

Subbarao [2] indicated that zirconia can be stabilized in the fluorite-type cubic phase when it is alloyed with an appropriate amount of di- or trivalent oxides of cubic system, such as CaO, MgO, R_2O_3 (R=rare earth), Y_2O_3, or Sc_2O_3 with overall composition MO_{2-x}, where $0<x$ mol%[1]<40. These oxides exhibit a relatively high solubility in ZrO_2 and are able to form fluorite-type phases which are stable over a wide range of composition and temperature. Yttria (Y_2O_3) is believed to be an excellent stabilizing additive for zirconia because of its high melting temperature (2435°C) and chemical inertness which make it of special interest for use at elevated temperatures [4]. Chistyi et al. [5] reported that crystals of yttria-stabilized zirconia possess high index of refraction, hardness, strength, and stability against oxidation at high temperatures (2500°C).

---

[1]In this thesis, mol% will be written m/o.

(a)

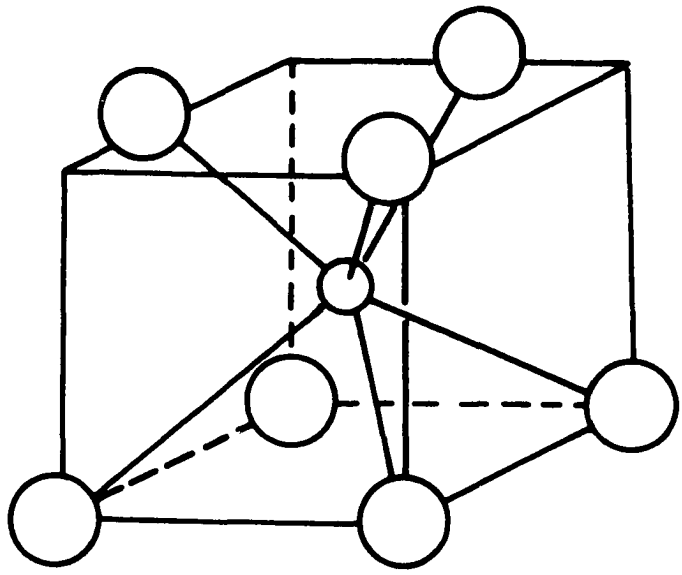

(b)

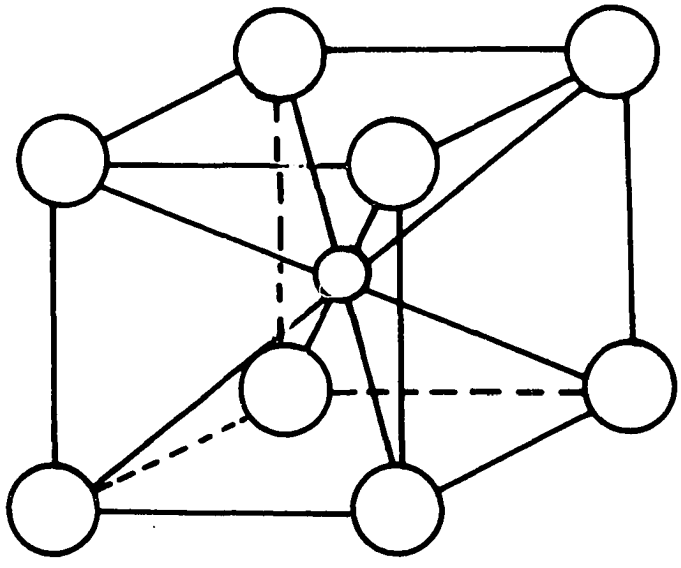

Figure 2. Oxygen coordination polyhedra; (a) idealized MO_7 group characteristic of ZrO_2 and (b) basic fluorite MO_8 group

Yttria possesses the cubic rare earth C-type structure [4]. This structure is most conveniently thought of as a modified fluorite structure where Y^{3+} occupies the center of a distorted cube. Fig. 3 shows the ideal spatial relations for two such cubes within the unit cell. In this structure, only 6 cube corners are occupied by oxygen ions. The unoccupied cube corners are on a face diagonal in one cube and on a body diagonal in the edge-adjacent cube. The fluorite (CaF_2) structure of YSZ is fcc, with space group Fm3m [4] (Fig. 1).

Wagner [6] established that stabilized zirconia contains oxygen ion vacancies. In YSZ, the oxygen vacancies are generated upon the substitution of Y^{3+} for Zr^{4+} cations according to the reaction

$$Y_2O_3 \rightarrow 2Y'_{Zr} + 3O^x_O + V_{\ddot{O}} \qquad (1)$$

Subbarao [2] indicated that Coulomb attraction between the two oppositely charged species (Y'_{Zr} and $V_{\ddot{O}}$), together with the large concentration of oxygen vacancies, would interfere with a random distribution of Y^{3+} ions over cation sites and vacancies over anion sites. Such materials are said to possess the 'defect' or 'disordered' fluorite structure. Hund [7] described the order-disorder reactions in YSZ by a complete cationic sublattice with anion vacancies. In the present study, the measurement of lattice

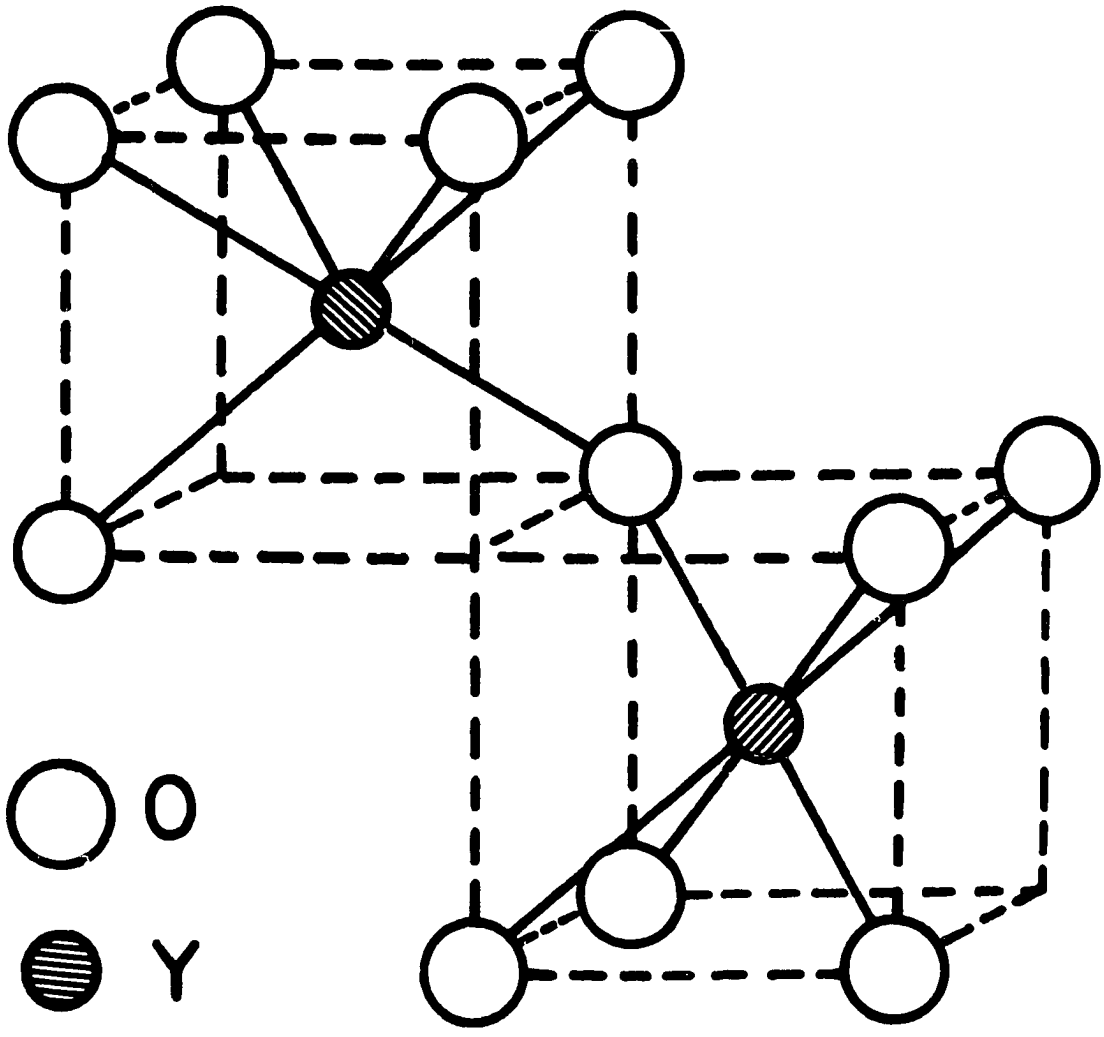

Figure 3. The C-type rare earth oxide structure and the six-fold coordination in Y_2O_3

constants and calculations of densities for YSZ crystals corroborate Hund's results. Morinaga et al. [8, 9], with x-ray diffraction on a crystal containing ~ 12 m/o Y_2O_3, found both the anions and cations were displaced slightly from the ideal positions; the oxygen ions were displaced along <100> directions and cations were displaced to a lesser degree along <111> directions. The lattice energy is minimized by anion lattice relaxation around the oxygen vacancies.

Intermediate between the fluorite (MO_2=M_4O_8) structure and the C-type (M_2O_3=M_4O_6) structure lies the pyrochlore (M_4O_7) structure [10]. The pyrochlore structure may also be thought of as a distorted fluorite with one-eighth of the anions missing. It differs from the fluorite structure by having the Y and Zr cations occupying alternating fluorite cation positions with an ordered arrangement of the vacant anion sites resulting in two kinds of coordination groups, AO_8 and BO_6.

1.2. Phase Relationships in ZrO_2-Y_2O_3 System

Several investigations have been made of the phase relationships in the zirconia-yttria system [11-17]. However, the definition of the phase fields, particularly at low temperatures, is uncertain, and indeed, even the number and character of the phases are questionable. Represen-

tative examples of phase diagrams which have been proposed are shown in Fig. 4 [11] and Fig. 5 [12], and differences are obvious.

The following comments pertain to aspects of the phase diagram which are relevant to observations in the present work. First, there are disparities in defining the limits of the YSZ phase field. The width of the phase field at room temperature extends from 7 [13], 9.9 [11], or 10 m/o Y_2O_3 [12] to ~14.5 [12], ~49.5 [11], or 55 m/o Y_2O_3 [13]. At higher temperatures, the fluorite phase field broadens and it seems reasonably established that on the ZrO_2-rich side the YSZ phase field extends to pure ZrO_2 above ~2380°C [11, 12, 14]. On the yttria-rich limit, however, there is a considerable amount of uncertainty. Stubican et al. [14] found a eutectoidal decomposition below 400°C of a single fluorite phase of YSZ into monoclinic ZrO_2 and rhombohedral $Zr_3Y_4O_{12}$ with essentially no terminal solid solubility between either of the two phases. According to this result, the fluorite phase should not be an equilibrium phase at room temperature.

Fu-kang et al. [15] reported yet different results in the vicinity of room temperature and indicated the existence of a two-phase field between a monoclinic terminal solution and a cubic pyrochlore ($Zr_2Y_2O_7$) at 33.33 m/o

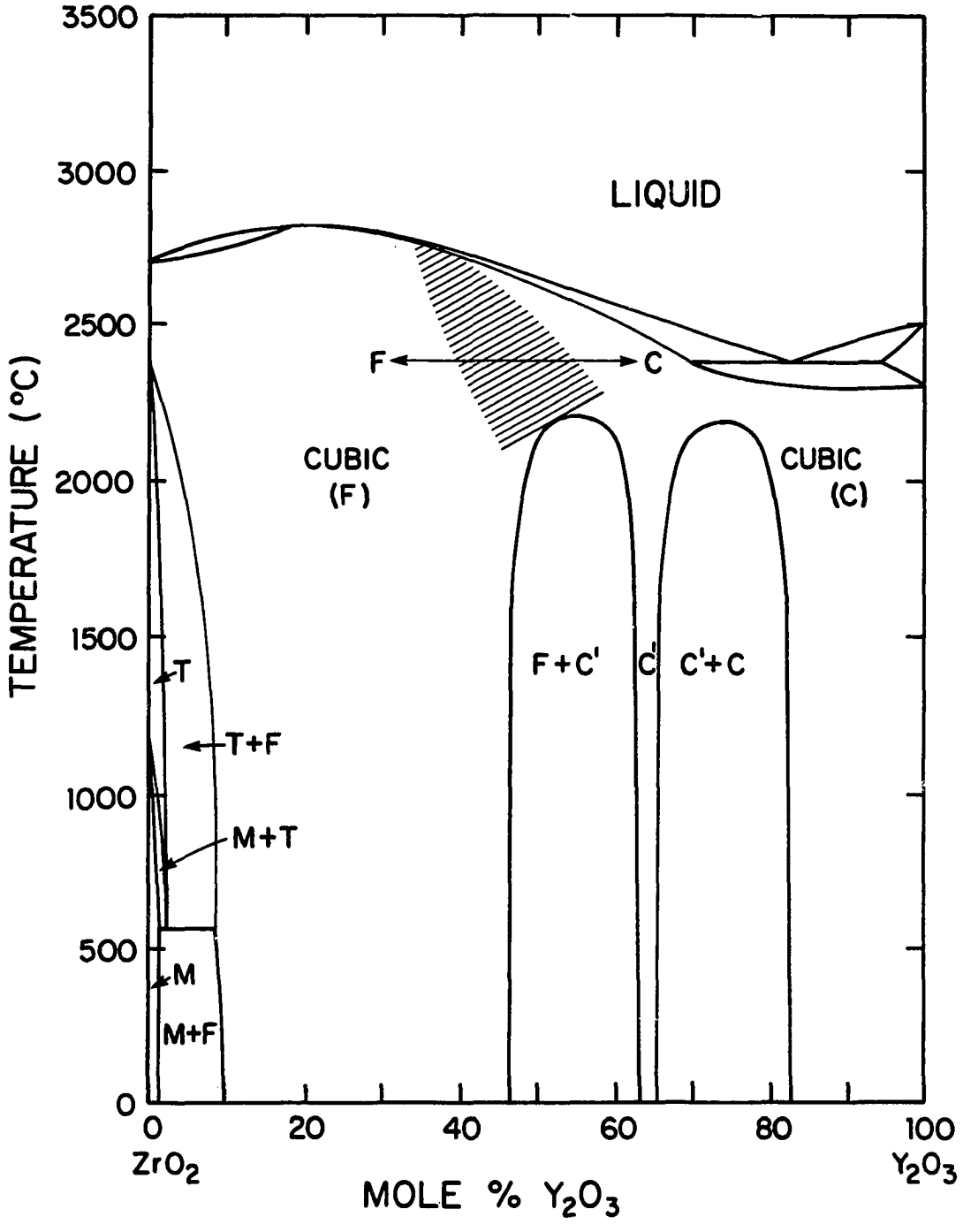

Figure 4. ZrO_2-Y_2O_3 phase diagram according to Scott [11]

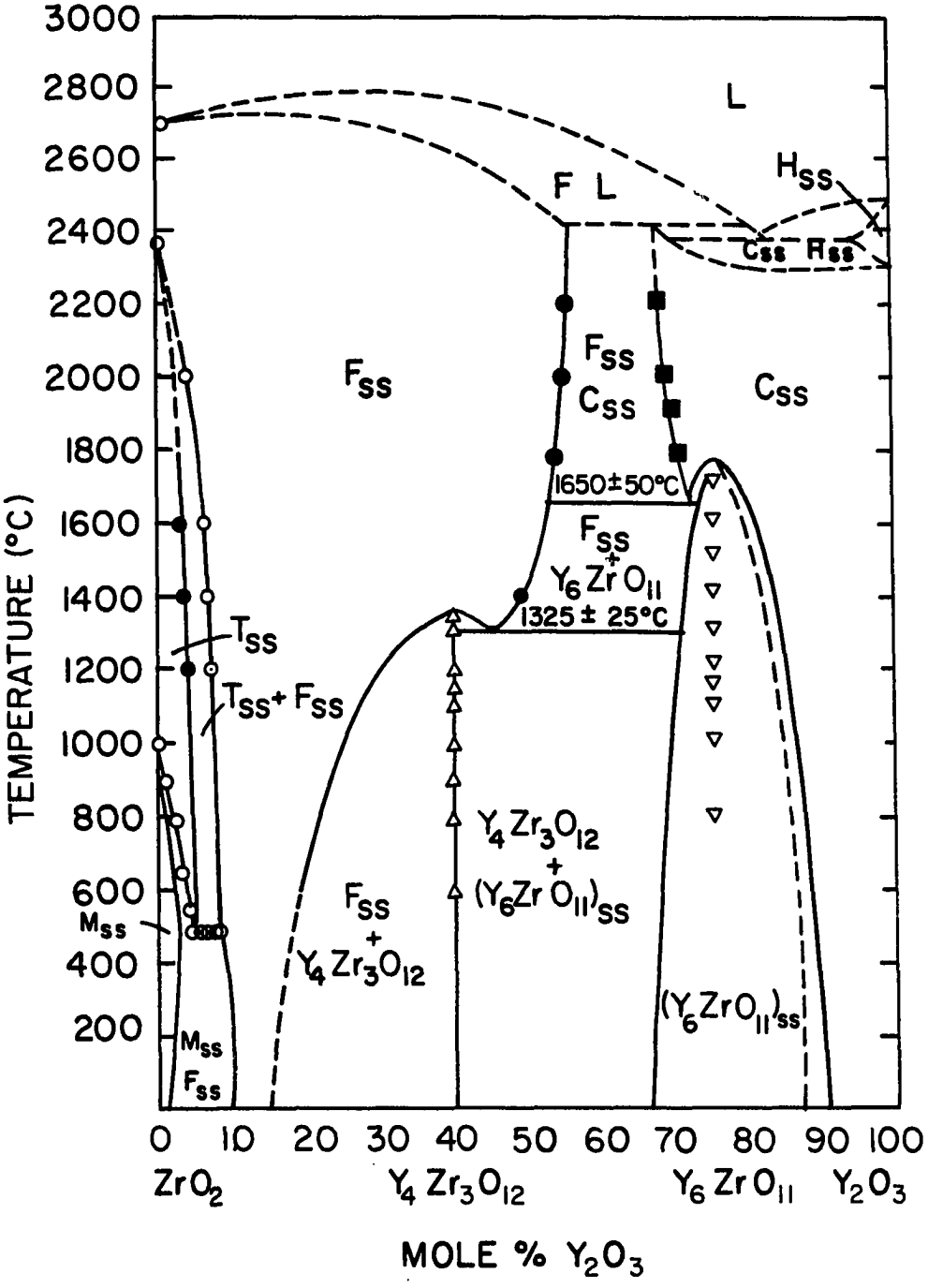

Figure 5. ZrO_2-Y_2O_3 phase diagram according to Pascual and Duran [12]

Y_2O_3. His published diagram must be considered schematic since it contains violations of the phase rule. Fu-kang et al. [15] reported the intermediate compound $Zr_2Y_2O_7$ remaining stable to temperatures as high as 2500°C. The existence of the pyrochlore structure has not been corroborated [14, 16], rather, most investigations [12, 14, 16, 17] have found the first intermediate phase to be $Zr_3Y_4O_{12}$ with a rhombohedral symmetry at 40 m/o Y_2O_3. This ordered phase is stable between room temperature and 1375°C.

Kinetic factors inhibit equilibrium at low temperature, which seems responsible for the discrepancies found among different reports. As an example, Scott [11] found that samples containing more than 8.1 m/o Y_2O_3 were single phase with fluorite structure at room temperature, but heating above ~80°C caused the appearance of a second phase. Samples with less yttria were two phases: one phase was monoclinic while the other was either fluorite or tetragonal, depending on the equilibration temperature. Peculiar behavior at a composition of 8.1 m/o Y_2O_3 has also been found in the present investigation. More details will be included in the discussion of the unusual elastic behavior of the 8.1 m/o Y_2O_3 crystal.

1.3. Elasticity and Wave Propagations in Crystals

The ultrasonic wave velocities in a material can be related to the elastic constants through a combination of Hooke's law and Newton's second law. A treatment of the elasticity theory and of the relationships of ultrasonic wave velocities to elastic constants can be found in a number of books, e.g., Kittel [18]. In cubic crystals there are three independent elastic constants, namely C_{11}, C_{12} and C_{44}. Propagation of waves in the [110] direction maximizes the resolution of the constants. Each ultrasonic wave velocity is related to an elastic constant through the relation

$$\rho V^2 = C_{ij}, \qquad (2)$$

where ρ is the crystal density, and C_{ij} is an appropriate combination of the elastic constants to be associated with the specific polarization and direction of the ultrasonic wave velocity, V. A summary of the elastic constants associated with different wave modes in cubic crystals is given in Table 1.

The elastic constants determined by ultrasonic methods are adiabatic because there is no time for heat exchange with the surroundings.

Table 1. Summary of wave mode-elastic constant relations in cubic crystals

Mode	Type	Propagation direction	Polarization direction	Velocity nomenclature	Elastic Constant
1	Longitudinal	[110]	[110]	$V_{L[110]}$	$(C_{11}+C_{12}+2C_{44})/2=C_L$
2	Shear	[110]	$[1\bar{1}0]$	$V_{T1[1\bar{1}0]}$	$(C_{11}-C_{12})/2=C'$
3	Shear	[110]	[001]	$V_{T2[001]}$	C_{44}
4	Longitudinal	[001]	[001]	$V_{L[001]}$	C_{11}
5	Longitudinal	$[1\bar{1}0]$	$[1\bar{1}0]$	$V_{L[1\bar{1}0]}$	$(C_{11}+C_{12}+2C_{44})/2$
6	Shear	$[1\bar{1}0]$	[110]	$V_{T[110]}$	$(C_{11}-C_{12})/2$
7	Shear	$[1\bar{1}0]$	[001]	$V_{T[001]}$	C_{44}
8	Longitudinal	[111]	[111]	$V_{L[111]}$	$(C_{11}+2C_{12}+4C_{44})/3$

1.4. Single Crystal Elastic Constants of YSZ

Data for elastic constants for single crystals of YSZ were available only at room temperature [5, 19-21] and below [22, 23]. Because of the high Debye temperature of this material, the elastic constants below room temperature are essentially temperature independent. The major uses of YSZ are at temperatures well above room temperature. On this basis, the present investigation was undertaken in order to provide elasticity data for the higher temperature region. The lack of agreement among the previous measurements was another reason for the present study.

2. EXPERIMENTAL PROCEDURES

2.1. Sample Preparation and Characterization

Single crystals of YSZ of five different compositions were obtained for the present investigation. One crystal was made available by Singh Industries, Inc. of Randolph, N.J., and the method of its preparation is not known to the author. The other four crystals were purchased from Ceres Corp. of Waltham, Massachusetts. The latter four crystals were grown from the melt by the technique of RF melting in a cold container [24]. In this technique, high-purity grades of ZrO_2 and Y_2O_3 are thoroughly mixed and put in a cylindrical container with metallic zirconium at the bottom of the container to act as heat inductor. The RF generator is turned on and when the melt reaches the surface, after about 5-10 min, additional portions of the oxides powder are gradually poured into it. The process of melting progresses gradually, the molten zone increases, and simultaneously intensive oxidation of the metal occurs which takes 10-15 min to be complete. The system is kept at constant power for 20-30 min to achieve equilibrium. Then, the container is slowly lowered at a rate of 10-30 mm/hr.

Preliminary orientation of the crystals was done with x-ray diffraction, and five specimens were cut from the 'as

grown' crystals with a diamond saw. Refinement of the crystallographic orientation of these five specimens was done with a back-reflection Laue technique [25]. Intermediate hand lapping on 600 grit abrasive paper brought the normals to the crystal faces within ±1° of the desired directions. All crystals were rectangular prisms with edge dimensions varying from 0.6-1.5 cm. Each of the crystals had two faces normal to the [001] direction, two normal to the [110] direction, and the last two normal to [1$\bar{1}$0]. Each of the opposite faces were made parallel within ±0.0003 cm. The dimensions of the crystals and the analytical composition are given in Table 2. Both zirconium and yttrium contents of the specimen crystals were determined utilizing a titrametric method [26]. The precision of the analyses is within ±0.04 m/o.

All crystals were checked for the presence of any second phase using a Picker θ-θ powder diffractometer with the internal standard (LiF) method at room temperature. Each diffraction pattern was fully identified as a single phase pattern belonging to the fcc fluorite structure.

Lattice parameter measurements were carried out at room temperature on small segments of ~0.1 mm in size taken from

Table 2. Compositions and dimensions of YSZ crystals

Crystal	Composition (±.04 m/o) Y_2O_3	ZrO_2	Thickness (±.0003 cm) [110]	$[1\bar{1}0]$	[001]
1	8.13	91.87	0.7297	0.9487	1.0269
2	11.09	88.91	1.3884	1.5088	1.4173
3	12.08	87,92	1.1707	0.9533	1.1412
4	15.52	84.48	0.9235	1.2713	1.2065
5	17.88	82.12	0.8115	0.6772	0.5720

the crystals during the orientation process. Using the Ames Laboratory-built-4-circle diffractometer and an automated indexing routine on a PDP-15 computer, nine high-angle reflections were used in evaluating lattice constants within ±0.006 A. The measured lattice constant was used, together with bulk density, to emphasize the mechanism of solid solution in the crystals. The bulk density was determined at room temperature by Archimedes principle within ±0.013 g/cc according to the ASTM Standard C-135-66. Table 3 gives the measured and calculated densities and the measured lattice constants of the crystals.

2.2. Ultrasonic Measurements

The pulse-echo-overlap technique [27-29] was used to measure both longitudinal and shear wave velocities. The longitudinal and shear waves were generated, respectively, by x-cut and y-cut single-crystal quartz transducers resonant at 10 MHz. A schematic diagram of the ultrasonic pulse-echo-overlap apparatus is shown in Fig. 6.

Velocities were measured by measuring the transit times between echoes from unrectified pulses traveling through crystals of known dimensions. The measurement of travel time, t, between two echoes is accomplished by setting the period 1/f of an electrical oscillator (oscillator

Table 3. Lattice constants and densities of YSZ crystals

Crystal	Y_2O_3 (m/o)	Lattice Parameter ±0.006 (Å)	Theoretical density (g/cc)	Bulk density ±0.013 (g/cc)
1	8.1	5.132	6.014	6.011
2	11.1	5.145	5.953	5.945
3	12.1	5.146	5.944	5.932
4	15.5	5.153	5.904	5.868
5	17.9	5.162	5.861	5.829

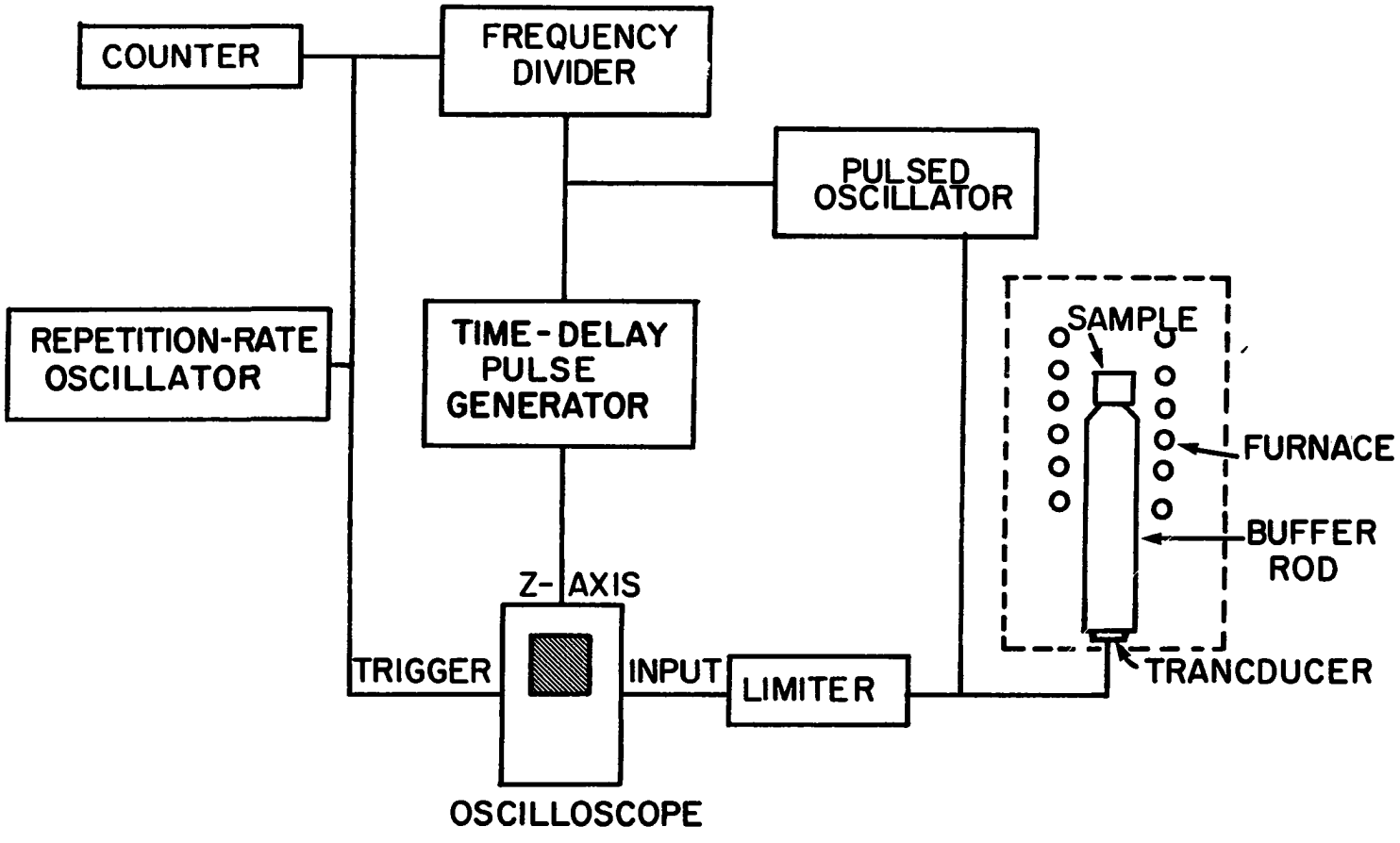

Figure 6. Block diagram of the ultrasonic pulse-echo-overlap apparatus

controlling an oscilloscope sweep) equal to the travel time, t, so

$$t = 1/f \quad \text{and} \quad f = 1/t \tag{3}$$

This adjustment causes successive echoes to be positioned one on top of the other on the oscilloscope. Overlapping can be adjusted by eye to ~±0.1 wavelength. The precision of measurement of an individual ultrasonic wave velocity is ~0.1%, which reflects a precision of ~0.2% into the elastic constant associated with this velocity.

In the present investigation, measurements above room temperature made necessary the employment of a low-attentuation fused silica buffer rod [30, 31] because quartz transducers lose their piezoelectricity at ~200-250°C. Fused silica rods of 14 cm in length and 2.4 cm in diameter were used with their ends made parallel within ±0.001 cm by a surface grinding technique. Two modifications were added to the buffer rod to eliminate the small parasitic echoes appearing in the main echo train due to mode conversion at the rod boundaries. Beveling one end of the buffer rod [32] supporting the specimen crystal and sanding the surface of the rod with a coarse abrasive paper provided relatively clean undistorted echo patterns for both longitudinal and shear modes. The buffer rod was kept in a vertical position with its higher end sealed to the specimen crystal with

AgCl, and the crystal was positioned in the uniform temperature zone of a resistance furnace. The other end of the rod was silvered and bonded to a quartz transducer and jacketed in a water-cooled coaxial holder. Longitudinal wave transducers were bonded with Nonaq stopcock grease and shear wave transducers with Salol (phenyl salicytate). Temperatures were measured within ±2°C with a Pt/Pt±13% Rh thermocouple spot welded to a platinum jacket enclosing the specimen crystal. Velocity measurements were carried out while heating and cooling the system. A schematic representation of the arrangement is shown in Fig. 7. With this arrangement ultrasonic wave velocities could be measured for a shear wave between room temperature and the melting point of the AgCl seal at ~455°C and for a longitudinal wave up to the furnace limit of 700°C. The fusion process of the AgCl bond affected the measurements by changing the slope of the velocity-temperature curves around 455°C. This effect was corrected by using another bond material. A eutectic salt of 53.5 m/o AgCl-46.5 m/o AgI, which melts at ~264°C, was used [33].

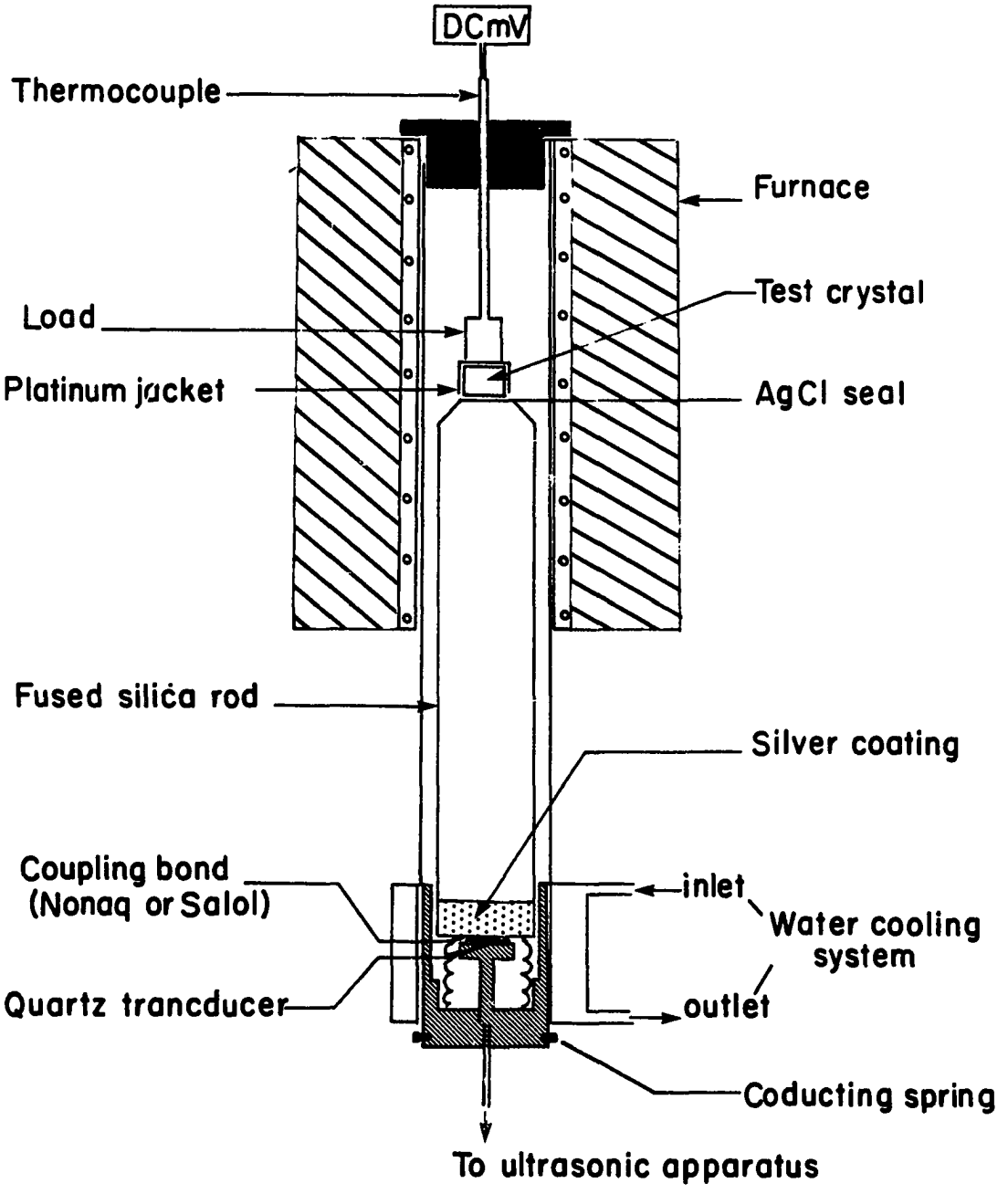

Figure 7. Experimental arrangement of ultrasonic wave velocity measurements above room temperature

3. RESULTS AND DISCUSSION

The elastic constants of YSZ crystals were calculated from ultrasonic velocities and bulk density. Room temperature values of constants C_{11}, C_{12} and C_{44} in the present study are compared with previous data by other investigations [5, 19, 21-23] in Table 4. Agreement in most cases may be noted to be within 5%; exceptions are C_{12} of the 12 m/o Y_2O_3 crystal [22] and those numbers which are listed in parentheses [5]. The disparity in the latter values results from the fact that crystal orientations deviated from normal mode directions by amounts of up to 5°. Differences in density and composition also contribute to the differences in values.

The compositional variations of the room temperature elastic constants from this investigation are shown in Fig. 9, where increasing Y_2O_3 concentration decreases C_{11} while C_{12} and C_{44} increase. The compositional dependencies of C_{11} and C_{44} at room temperature agree with the results of Chistyi et al. [5] and Aleksandrov et al. [20], but the compositional dependence of C_{12} varies from one investigation to another. In the present work, C_{12} increases with Y_2O_3 content, Chistyi found C_{12} to be composition independent, and Aleksandrov found a minimum value of C_{12} at ~14 m/o

Table 4. Comparison of room temperature elastic constants for YSZ crystals with literature data

Y_2O_3 (m/o)	Bulk Density (g/cc)	Elastic Constant (GPa) C_{11}	C_{12}	C_{44}	References
8	5.99	394	91	56	23
8	6.01	410	90	53	5[a]
		415	119	57	5[b]
8.1	6.011	405	95	56	This work[c]
10	5.95	382	108	60	19
10	5.95	(395)	(117)	(61)	5[d]
10.3	5.91	403	83	58	21
11.1	5.945	403	102	60	This work
12	5.894	449	55	62	22
12	5.89	403	100	57	5[a]
		385	108	59	5[b]
		(391)	(71)	(60)	5[d]
12.1	5.932	405	105	62	This work
15.5	5.868	398	109	66	This work
16.5	5.81	390	96	61	5[a]
		379	106	67	5[b]
		(380)	(74)	(62)	5[d]
17.9	5.829	390	111	69	This work
20	5.76	(372)	(117)	(68)	5[d]

[a]Measurements of Brillouin scattering of light.

[b]Ultrasonic measurements.

[c]The temperature dependencies of the elastic constants of the 8.1 m/o Y_2O_3 crystal were not reproducible, although the room temperature constants were reproducible.

[d]Measurements on crystals with orientation uncertainties up to ±5° are shown in parentheses.

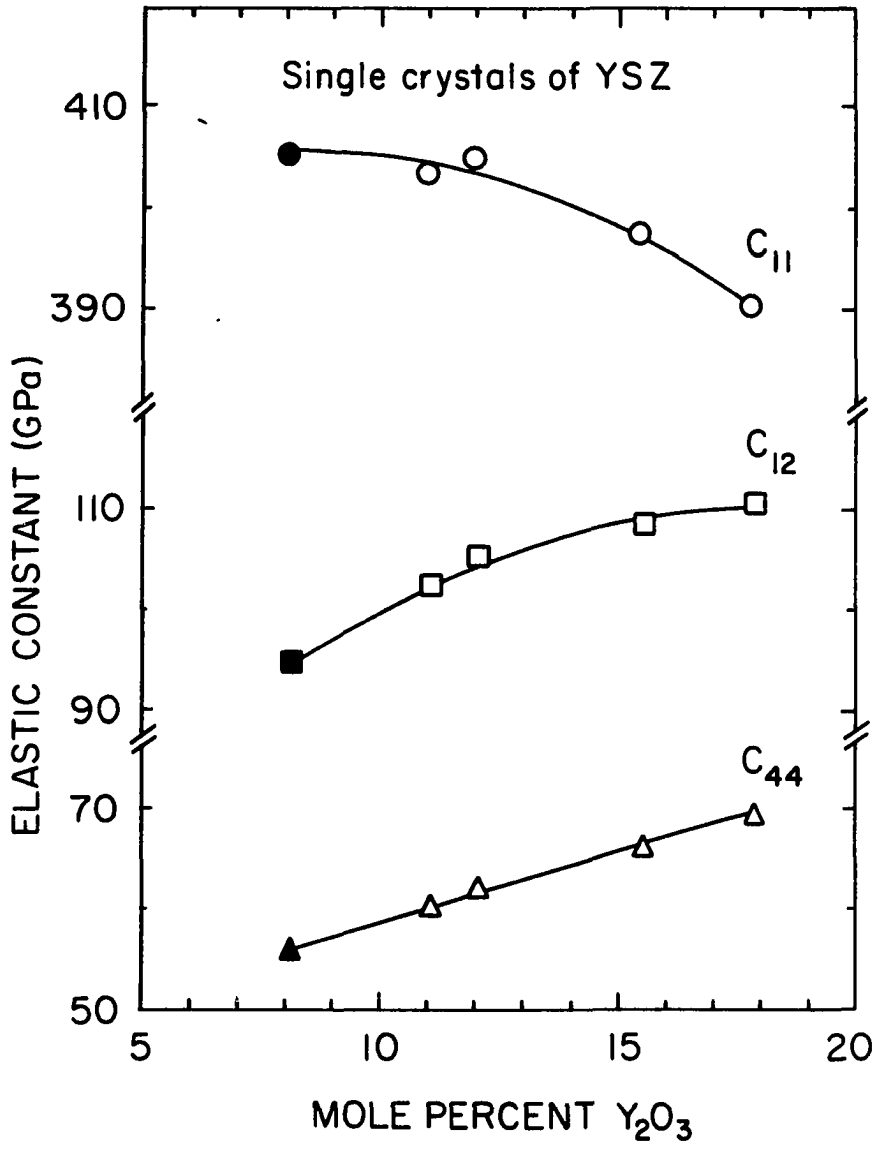

Figure 6. Compositional dependencies of C_{11}, C_{12} and C_{44} for YSZ crystals at room temperature. The solid symbols are used to differentiate the 8.1 m/o Y_2O_3 crystal from the others because the temperature dependencies of the elastic constants for this crystal were not reproducible, although the room temperature constants were reproducible

Y_2O_3. It should be emphasized that C_{12} is an off-diagonal element and is experimentally determined with poorer precision than either C_{11} or C_{44}.

To understand the compositional dependencies of C_{11}, C_{12}, and C_{44}, it is appropriate to consider the atomic interactions which control the elastic constants. Cochran [34] has considered the problem and has discussed various models for calculating the elastic constants of ionic and covalent crystals. Axe [35] and Srinivasan [36, 37] have looked explicitly at the fluorite structure and have derived expressions for the elastic constants assuming a shell model. Srinivasan's expressions are somewhat more general. In his representation, elastic constants are related to the microscopic forces between crystal ions. The general forms are:

$$C_{11} = \left(\frac{e^2}{a_o^4}\right) \left[-0.7628\ Z_c Z_a + \frac{1}{12}\ (A_1+2B_1) + \frac{1}{4}\ A_2\right] \qquad (4)$$

$$C_{12} = \left(\frac{e^2}{a_o^4}\right) \left[1.3511\ Z_c Z_a + \frac{1}{12}\ (A_1-4B_1) - \frac{1}{4}\ B_2\right] \qquad (5)$$

$$C_{44} = \left(\frac{e^2}{a_o^4}\right) \left[0.3814\ Z_c Z_a + \frac{1}{12}\ (A_1+2B_1) + \frac{1}{4}\ B_2 + 1\right] \qquad (6)$$

where e is the unit charge and a_o is the lattice parameter. In each constant, the first term comes from Coulomb forces, where Z_c and Z_a represent the ionic charges on

the cations and anions. A and B represent, respectively, the radial and tangential components of the short-range repulsive force interactions. The subscripts 1 and 2 denote first and second nearest neighbor interactions. The final term in C_{44}, I, is of lesser magnitude and involves all the previous contributions plus explicit shell-model parameters.

The most important contributions are the Coulomb forces and the short-range repulsive overlap forces of the first nearest neighbors. In the YSZ crystals, the Coulombic term, in contrast with the repulsive one, was found to be relatively stronger compositional function through changing Z_c and Z_a. A simple, although adequate, explanation of the repulsive contribution and its compositional dependence may be understood from the expression presented by Fuchs [38] of the Born-Mayer repulsive potential W(R) between two ions

$$W(R) = cb \exp [(r_1+r_2-a_o)/g] \qquad (7)$$

where c represents, according to Pauling [39], the dependence of the repulsive potential on the charge and the species of the ions, b and g are constants for a given crystal structure, r_1 and r_2 are the ionic radii, and a_o is the lattice parameter. In the YSZ crystals, since a_o

is a weak function of composition and the ionic radii of Y^{3+} and Zr^{4+} are comparable, the repulsive potential and its derivatives with respect to a_o would not be a strong function of decomposition.

In contrast to the weak compositional dependence of the Born-Mayer repulsive potential, the Coulomb energy and the Coulombic forces are appreciably composition dependent through the differing ionic charges of +4 for Zr and +3 for Y. References to Equations 4, 5 and 6 show that if the cationic charge is taken as weighted value of $Z_c=x(+3) + (1-x)(+4)$, with x being the fraction of cation sites occupied by yttrium and the corresponding anionic charge is taken as $Z_a=-Z_c/2$, then the constant C_{11}, C_{12}, and C_{44} are all composition dependent primarily through the compositional dependence of the Coulomb contribution. Further, the signs of Z_c and Z_a are opposite so the product Z_cZ_a is negative and therefore, the compositional dependence of C_{11} is negative and of C_{12} and C_{44} is positive. The room temperature values of the elastic constants of YSZ crystals are essentially the absolute zero temperature values since these constants are almost temperature independent below room temperature.

Debye temperature is an important parameter of a solid which can be evaluated from single crystal elastic

constants. It represents an average effect of vibrating masses and spring force constants defining elastic constants in the crystal lattice. Debye temperatures of the crystals were calculated at room temperature with the tables of Overton and Schuch [40] which list values of the function $G(S, \tau)$ for the relation

$$\theta_D = (3.3053 \times 10^{-11}) \left(\frac{N}{V}\right)^{1/3} \left(\frac{C_{44}}{\rho}\right)^{1/2} G(S, \tau) \qquad (8)$$

where N is the number of atoms per unit formula (equals 3 in the present case), V is the volume per formula weight $(a_o^3/4)$, and $G(S, \tau)$ is a function of the elastic constants with S and τ being determined from the relationships

$$S = \frac{C_{11}-C_{44}}{C_{12}+C_{44}} \quad \text{and} \quad \tau = \frac{C_{12}+C_{44}}{C_{44}} \qquad (9)$$

The results of the calculations are given in Table 5. Fig. 9 shows a linear relationship between Debye temperatures of the crystals at room temperature and the square root of the inverse masses per unit formula $Zr_{1-x}\ Y_x\ O_{2-x/2}$, with x being the fraction of cation sites occupied by yttrium. The linear relationship shown in Fig. 9 may be understood from considerations of lattice dynamics. At sufficiently low temperatures, Debye temperature is proportional to a characteristic cut-off frequency arising solely from acoustic vibrations [41]. In a harmonic approximation and with neglect of any change in force constants, this

Table 5. Debye temperatures of YSZ crystals at room temperature

Crystal	(Y/Zr) atom	x ($YO_{1.5}$)	m	(N/V) ($10^{22}cm^{-3}$)	S	τ	G(S, τ)	θ_D(K)
1	0.18	0.15	121.7	8.880	2.32	2.70	1.215	545.4
2	0.25	0.20	121.2	8.811	2.12	2.71	1.294	557.4
3	0.27	0.22	121.0	8.806	2.05	2.70	1.186	562.9
4	0.37	0.27	120.4	8.771	1.90	2.65	1.166	573.3
5	0.43	0.30	120.1	8.725	1.79	2.60	1.149	579.9

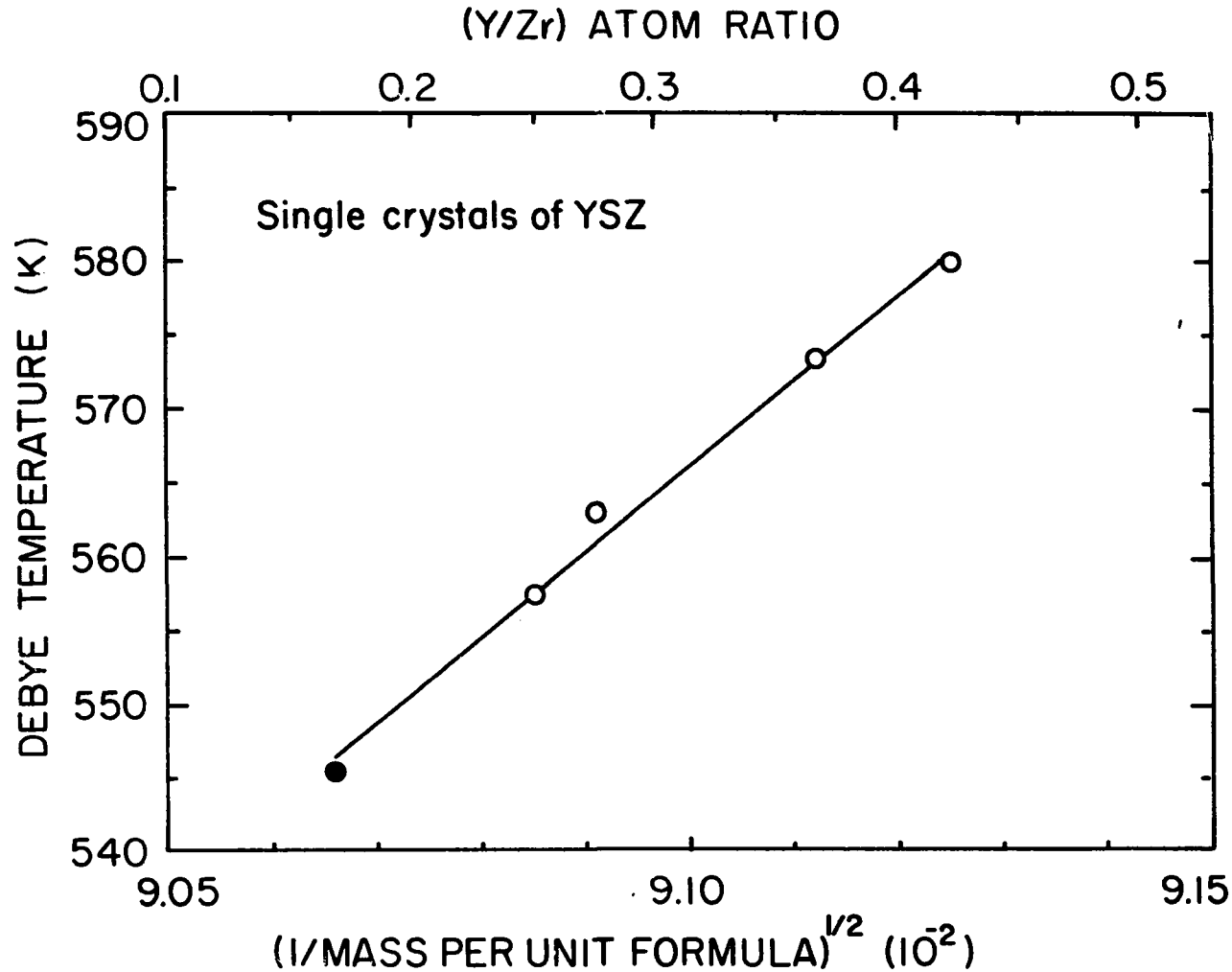

Figure 9. Variation of Debye temperatures of YSZ crystals with the square root of the inverse mass per formula at room temperature

characteristic frequency should be inversely proportional to the square root of the vibrating masses. The present results for Debye temperatures of the YSZ crystals parallel the reslts of Schannette and Smith [42] on single crystals of $ZrCo_2$ and $HfCo_2$.

Above room temperature, the elastic constants of the crystals show a regular decrease in magnitude with increasing temperature due to the combined effects of thermal expansion and anharmonicity. A lack of reproducibility was observed in the 8.1 m/o Y_2O_3 crystal in the sense that successive thermal excursions followed different paths. This behavior is illustrated in Fig. 10 where the longitudinal wave velocity $V_{L[110]}$ is plotted versus temperature and where the following points may be noted. First, the paths are not reproducible from run to run, although below ~300°C the behavior appears to be normal and the room temperature value is reproducible. Second, in the early runs, a and b, the heating and cooling behaviors follow the same paths in each run, but differ between runs. But, this is not true in runs c, d, and e, where the heating and cooling paths differ with difference increasing with increasing number of the run. The overall behavior is anomalous in the sense that if there is some degree of phase transformation it would not be expected that the room temperature value would be reproducible. In contrast, the

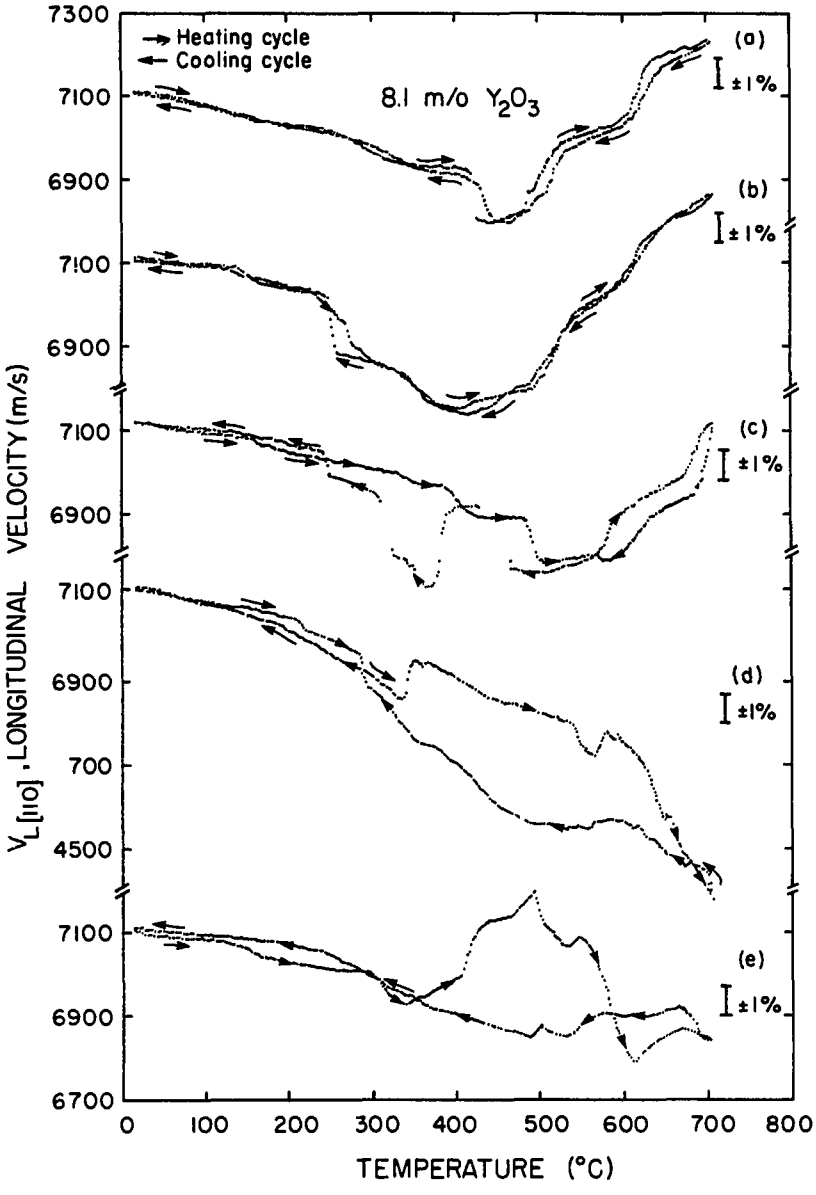

Figure 10. Temperature dependence of the longitudinal wave velocity $V_{L[110]}$ for the 8.1 m/o Y_2O_3 crystal, measured at different times; (1) initial measurement, (b) after 5 days, (c) after 2 weeks, (d) after 5 weeks, and (e) after 10 weeks

shear wave velocities $V_{T_1[1\bar{1}0]}$ and $V_{T_2[001]}$ show a regular decrease with increasing temperature in the range of measurements as shown, respectively in Figs. 11 and 12. However, the degree of reproducibility of each measurement varies with temperature. Surprisingly, the room temperature values of the constants C_{11}, C_{12} and C_{44} are reproducible within up to 0.5%.

At present, the behavior of the 8.1 m/o Y_2O_3 alloy is not understood and remains for future research to explain.

In contrast to the behavior of the 8.1 m/o Y_2O_3 crystal, the pure mode elastic constants of the other crystals show a regular decrease with increasing temperature. The constant C_{12} also softens with increasing temperature. These behaviors are reproducible in the temperature range of measurements. The temperature dependences of C_{11}, C_{12}, C_{44}, C', and C_L of different YSZ crystals are shown, respectively, in Figs. 13, 14, 15, 16, and 17.

AgCl melts at 455°C, therefore, shear measurements could not be obtained at higher temperatures where AgCl was used as a bonding material, whereas longitudinal measurements could be made to 700°C (furnace limit). In order to get some feeling of the temperature dependence of C' above the melting point of AgCl, the temperature dependencies of

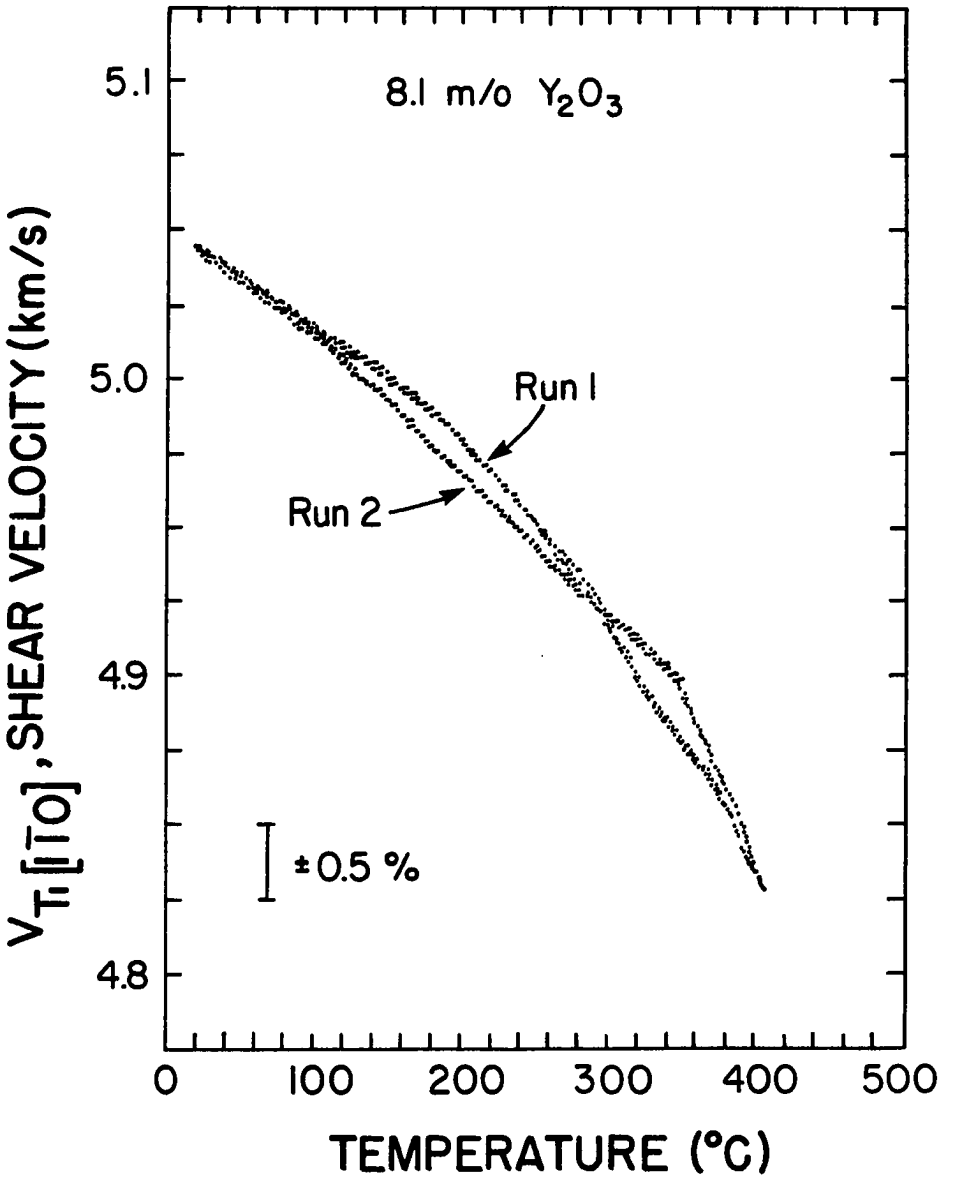

Figure 11. Temperature dependence of the fast shear wave velocity $V_{T1[1\bar{1}0]}$ for the 8.1 m/o Y_2O_3 crystal. Runs 1 and 2 were measured 10 weeks apart

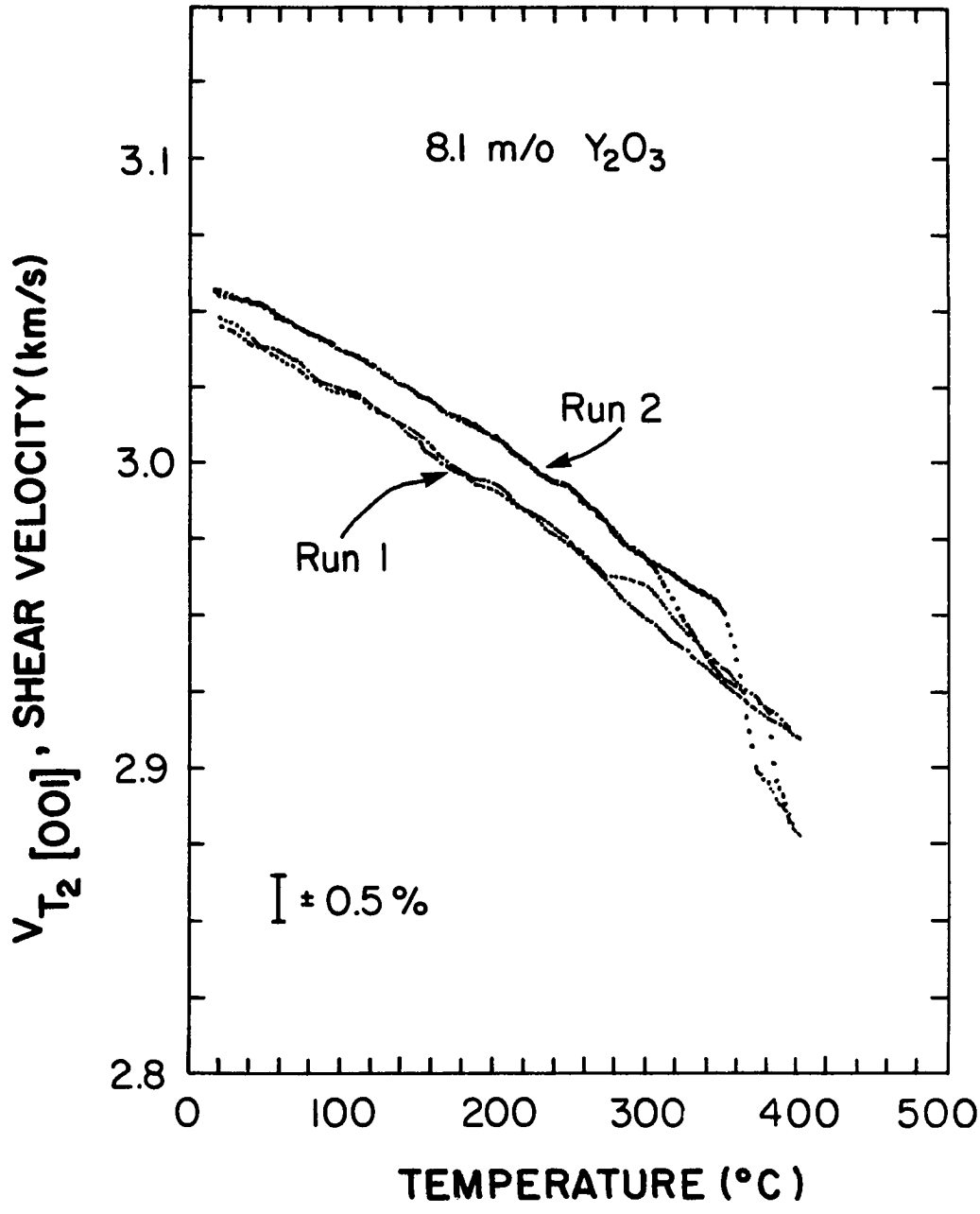

Figure 12. Temperature dependence of the slow shear wave velocity $V_{T2[001]}$ for the 8.1 m/o Y_2O_3 crystal. Runs 1 and 2 were measured 10 weeks apart

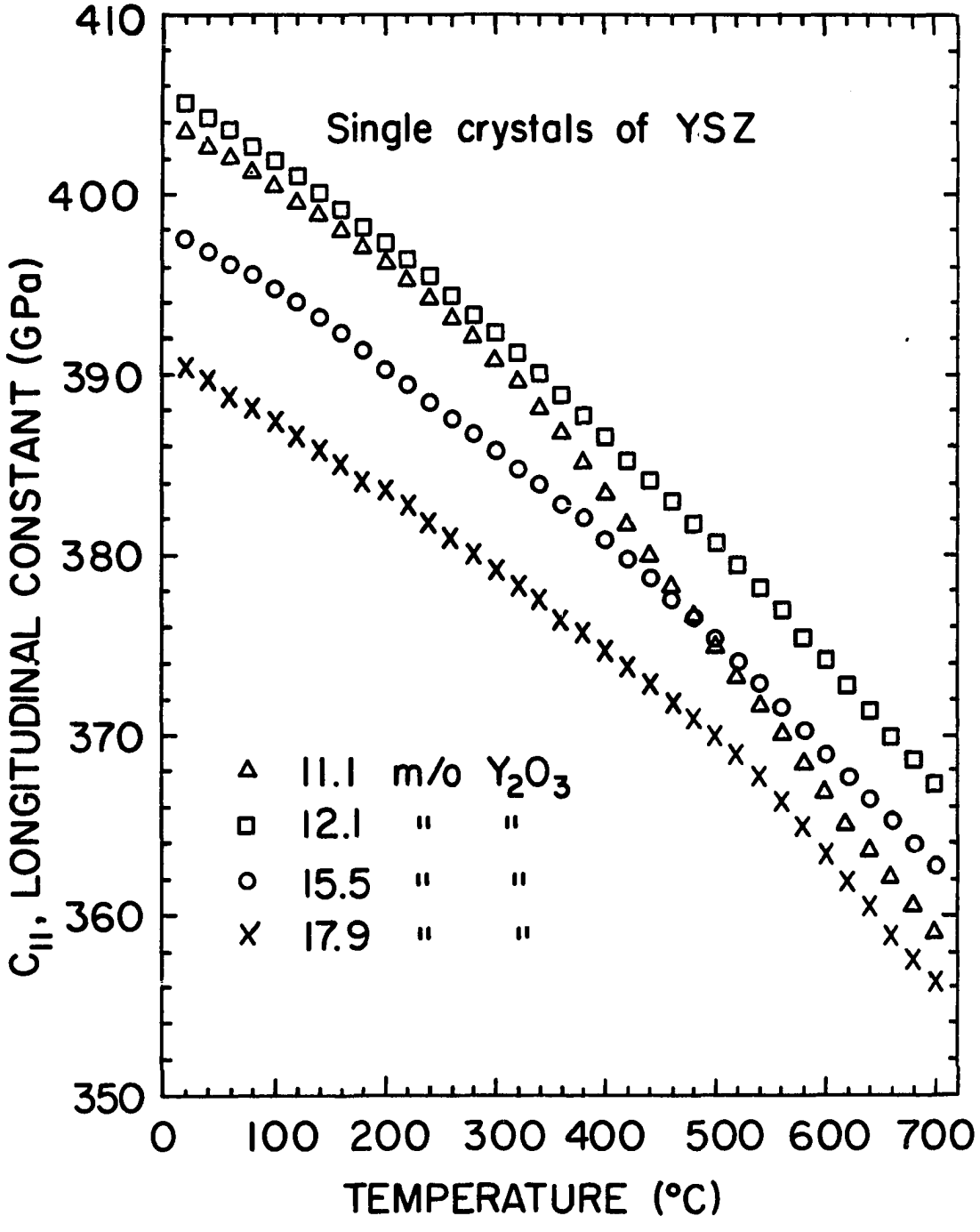

Figure 13. Temperature dependence of C_{11} for YSZ crystals

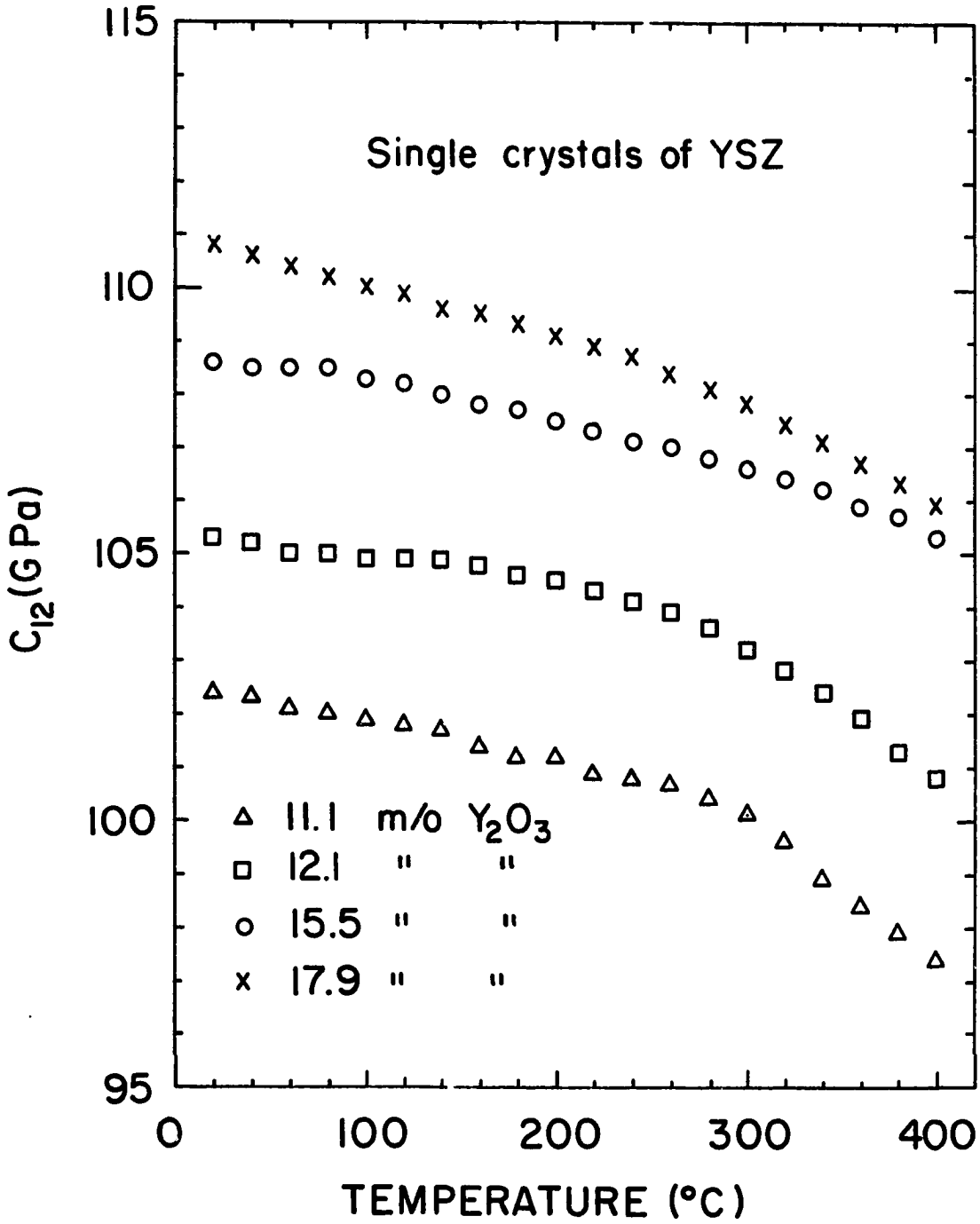

Figure 14. Temperature dependence of C_{12} for YSZ crystals

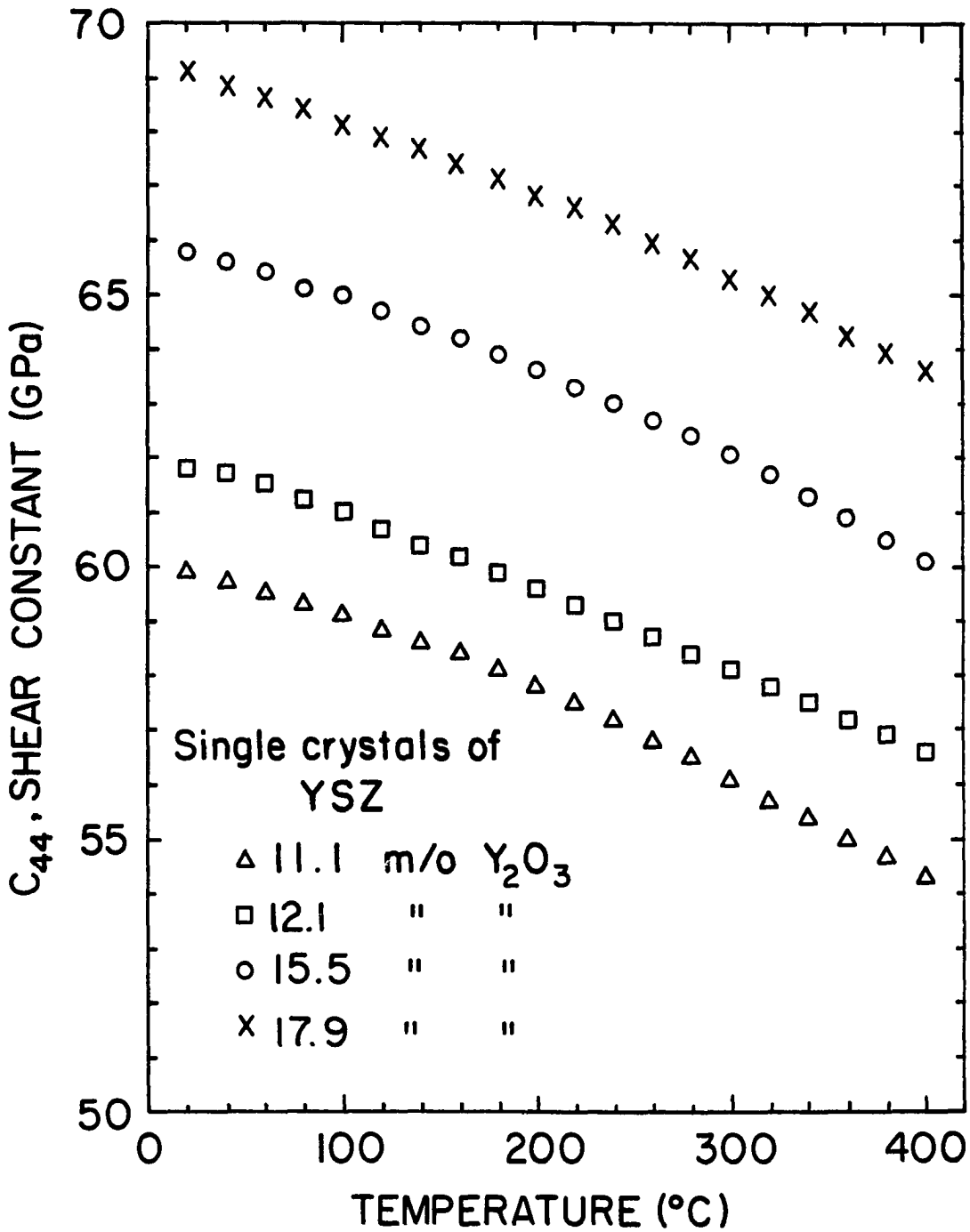

Figure 15. Temperature dependence of C_{44} for YSZ crystals

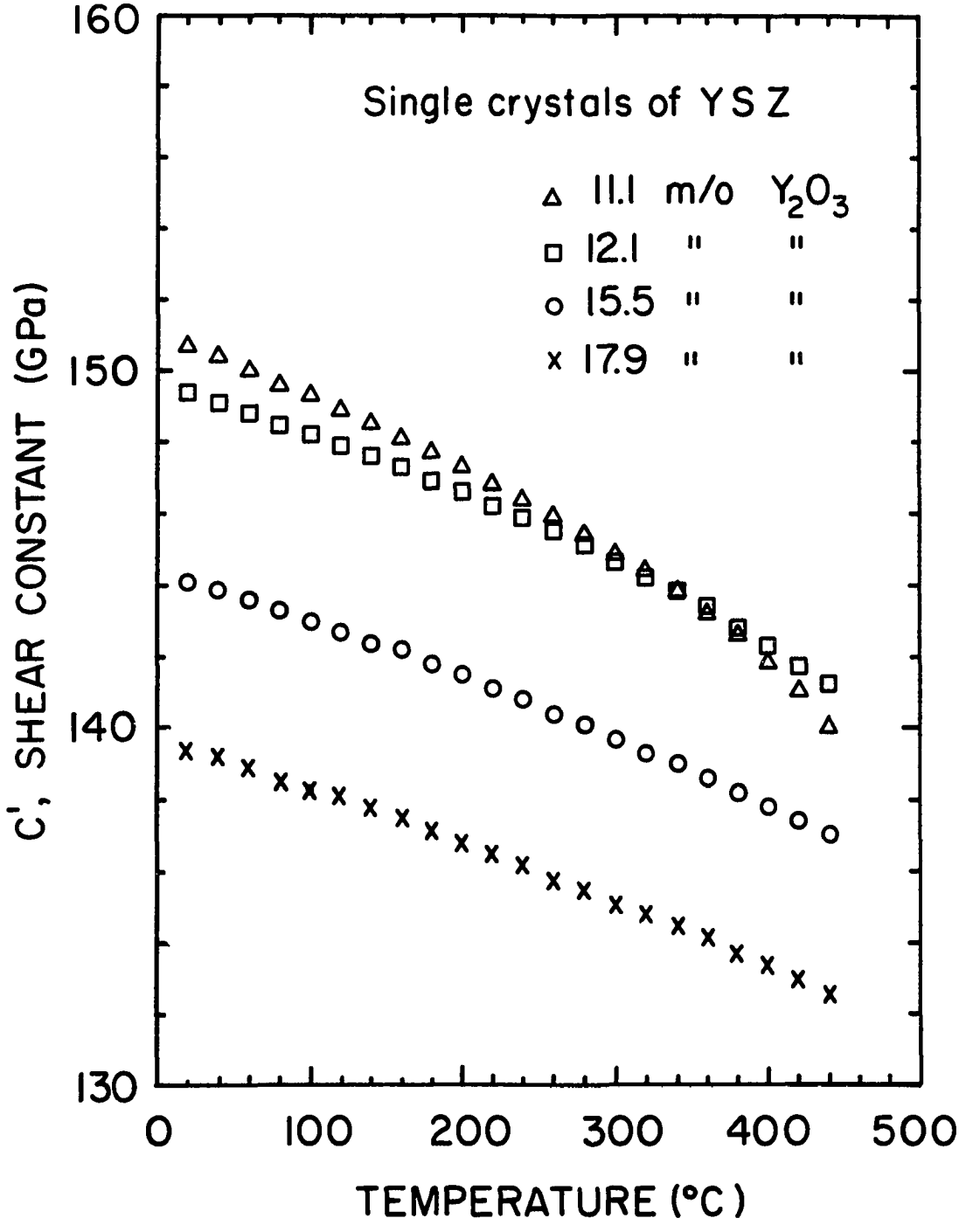

Figure 16. Temperature dependence of C' for YSZ crystals

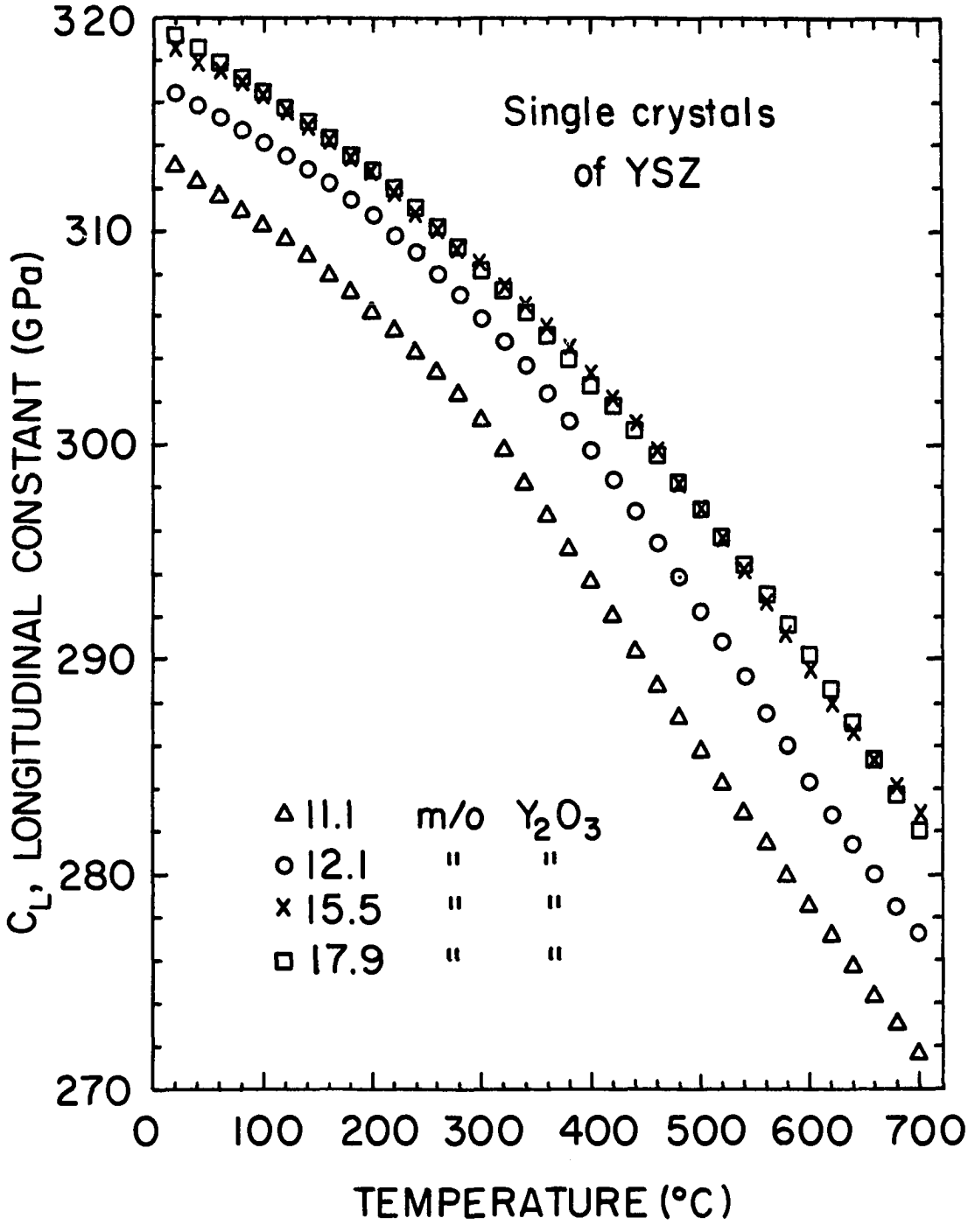

Figure 17. Temperature dependence of C_L for YSZ crystals

two longitudinal constants C_L and C_{11} were considered together with an extrapolation of C_{44} to 700°C. This extrapolation was justified on the basis that C_{44} behaves in a smooth monotonic manner throughout the temperature range of measurement. And, the C_{12} data above 440°C were evaluated from the relation

$$C_{12} = 2(C_L - C_{44}) - C_{11} \qquad (10)$$

Therefore, values of the three independent constants C_{11}, C_{12} and C_{44} were made available over the temperature range 20-700°C. Tables 9, 10, 11, and 12 in the Appendix give the values of elastic constants every 100°C for YSZ crystals, respectively containing 11.1, 12.1, 15.5, and 17.9 m/o Y_2O_3.

It may be noted that the temperature dependencies of C_{11}, C_{12} and C_{44} maintain the same compositional dependencies discussed previously. In Fig. 16, it is obvious that C' of the 11.1 m/o Y_2O_3 drops sufficiently rapidly with increasing temperature and it crosses C' of the 12.1 m/o alloy at ~320°C and continuing to decrease with increasing temperature. Although C' of the 11.1 and 12.1 crystals cross, they do not change the compositional dependence of shear anisotropy.

Shear anisotropy is reflected in the general elastic behavior of the crystal and is defined as

$$A = \frac{C_{11}-C_{12}}{2C_{44}} = \frac{C'}{C_{44}} \qquad (11)$$

The YSZ crystals possess a high degree of shear anisotropy (A=2.02-2.51) at room temperature. Shear anisotropy decreases linearly with increasing Y_2O_3 concentration but increases with increasing temperature, as shown in Fig. 18. The room temperature values of shear anisotropy agree within up to 9% with the result of Chistyi et al. [5] and Aleksandrov et al. [19-21].

Extrapolation of the linear compositional dependence of shear anisotropy at room temperature indicates that YSZ crystals would be elastically isotropic, i.e., A=1, at ~32 m/o Y_2O_3 composition. Surprisingly, this composition corresponds to the ordered phase $Zr_2Y_2O_7$ with a pyrochlore structure reported by Fu-Kang et al. [15] at 33.33 m/o Y_2O_3 which was proven not to exist [12, 14, 16, 17].

Longitudinal anisotropy is reflected in the tensile stiffness in a cubic crystal through the relation [43]

$$C_{\alpha_i, \alpha_j} = C_{11} - 2(C_{11}-C_{12}-2C_{44}) \left(\sum_{\substack{i,j \\ i\neq j}}^{3} \alpha_i^2 \alpha_j^2\right), \qquad (12)$$

where $C_{\alpha i, \alpha j}$ is a longitudinal constant associated with the direction specified by the direction cosines (α_i and α_j) between the measurement direction and the three

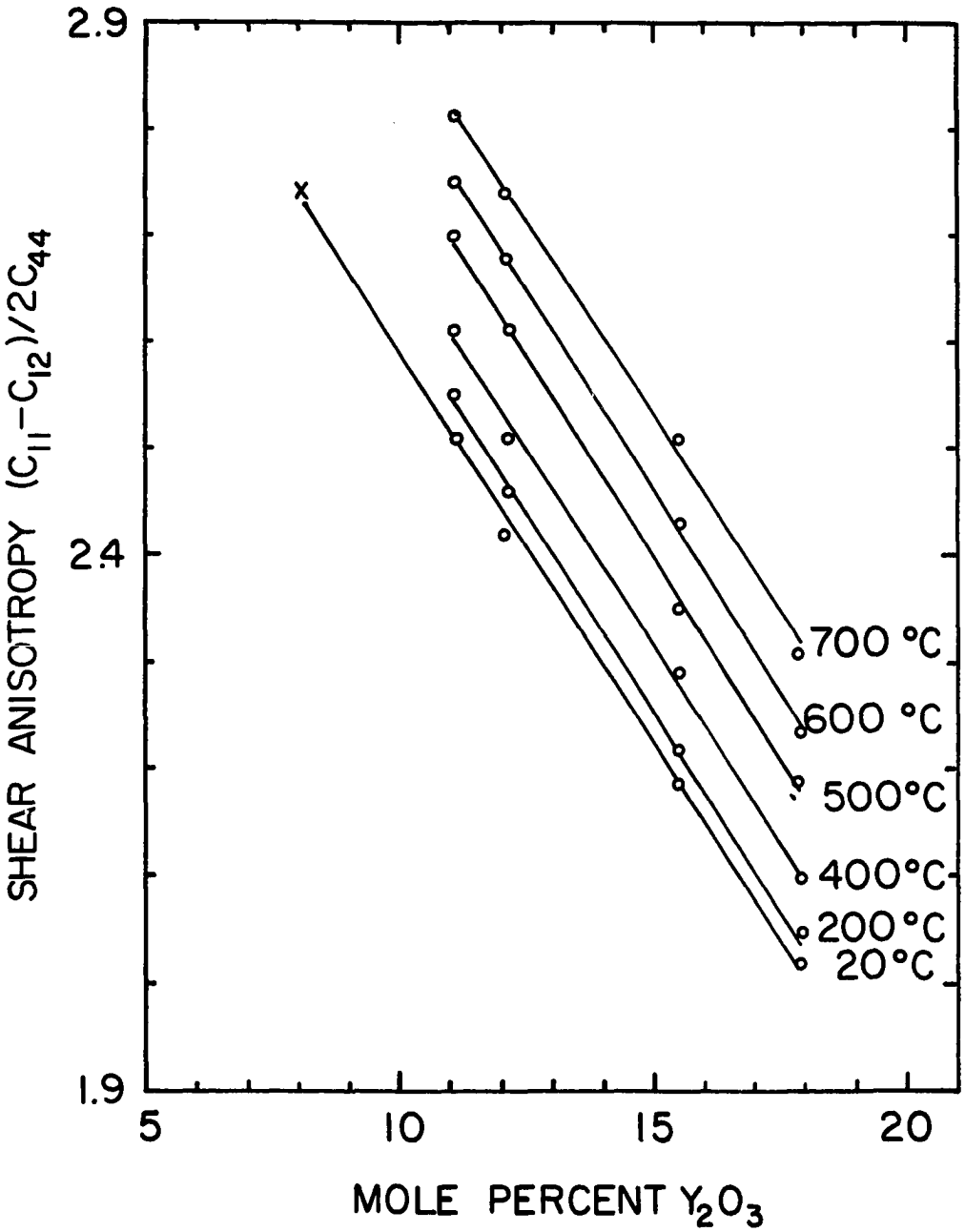

Figure 18. Variation of shear anisotropy with composition of YSZ crystals at different temperatures. The 8.1 m/o Y_2O_3 value is shown in a different symbol (x) for the same reason as before

crystallographic axes. It is found experimentally that the value of C_{11} is the maximum value for any longitudinal constant. This is consistent with Equation (12) because the term, $C_{11}-C_{11}-2C_{44}$, is positive. Thus, $C_{\alpha i,\alpha j}<C_{11}$ since $\sum_{\substack{i,j \\ i\neq j}}^{3}=0$ along axial directions and increases above zero for all other directions. Table 6 gives the longitudinal constants measured along [100] and [110] directions and calculated along [111] for the YSZ crystals at room temperature.

The compositional dependencies of the longitudinal constants along [100], [110], and [111] for the crystals at room temperature are linear when the constants are plotted on a log scale, as shown in Fig. 19. Increasing Y_2O_3 concentration was found to decrease the longitudinal constant along [100] while increasing the constants along [110] and [111]. Extrapolation of the linear correlations shows a crossing near 40 m/o Y_2O_3, indicating a longitudinal isotropy where a number of investigations [12, 14, 16, 17] have established the presence of an ordered phase $Zr_3Y_4O_{12}$ with a rhombohedral symmetry. The c-axis of the rhombohedral phase is the [111] cube diagonal of the fluorite phase [44]. Further, the rhombohedral structure of $Zr_3Y_4O_{12}$ can be described in a hexagonal representation which requires

Table 6. Variations of longitudinal and shear constants along different directions in YSZ crystals at room temperature

Y_2O_3	Log (Elastic Constant, GPa)				
	Longitudinal			Shear	
m/o	[100]	[110]	[111]	[100][a]	[110][b]
8.1	2.608	2.482	2.435	1.746	2.184
11.1	2.606	2.495	2.451	1.778	2.178
12.1	2.608	2.500	2.459	1.791	2.174
15.5	2.599	2.503	2.466	1.818	2.159
17.9	2.591	2.504	2.471	1.839	2.144

[a]Propagation in [100] and polarization in [010].

[b]Propagation in [110] and polarization in $[1\bar{1}0]$.

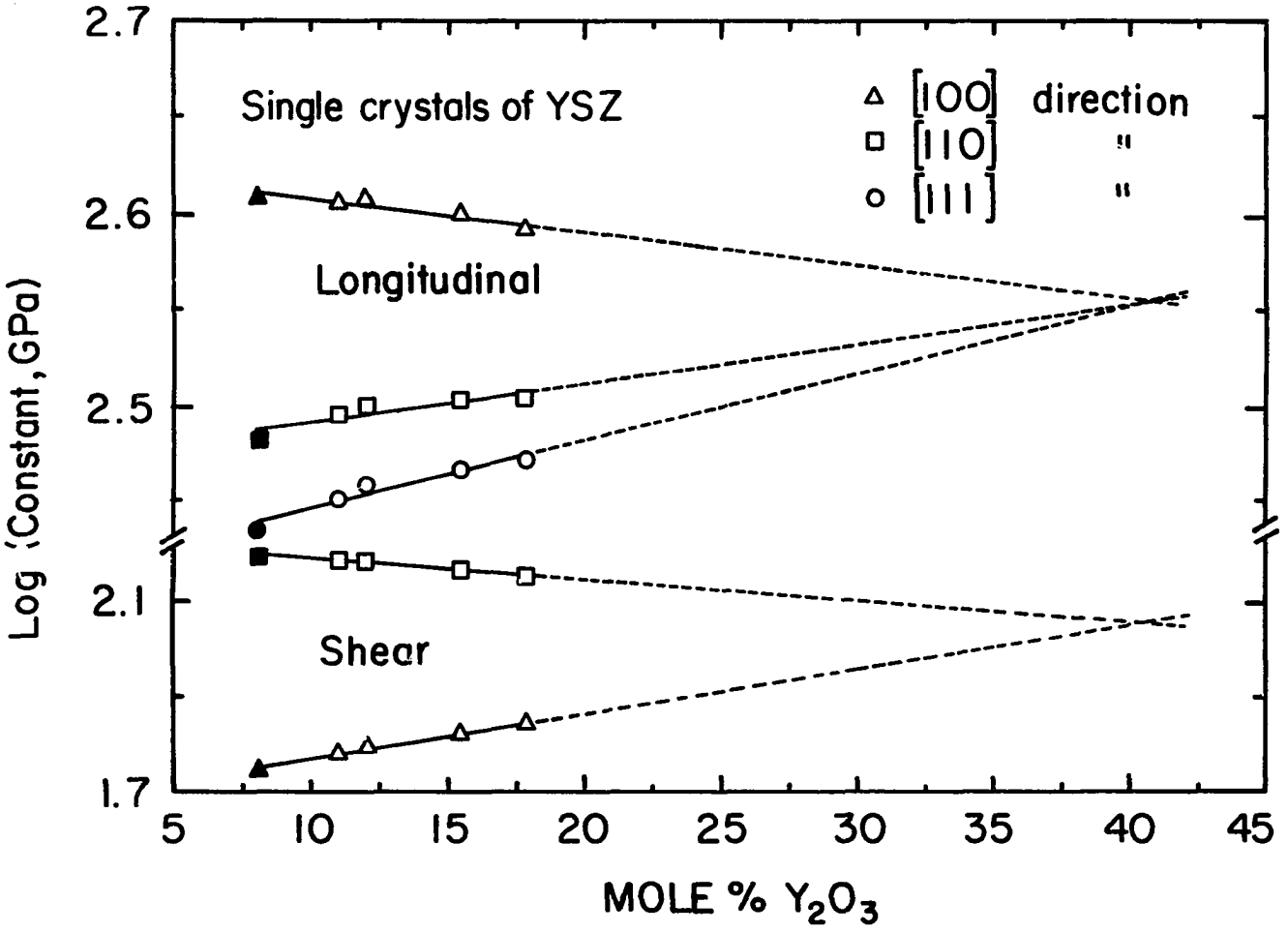

Figure 19. Variations of longitudinal and shear constants along different directions in YSZ crystals at room temperature. The 8.1 m/o Y_2O_3 values are shown in solid symbols for the same reason as before

cylinderical elastic symmetry [45]. Thus, if the structural change from cubic YSZ to rhombohedral $Zr_3Y_4O_{12}$ with increasing Y_2O_3 content can be viewed as a pseudo continuous ordering of Y and Zr ions, then the equality of C_{11} and C_L is required at stoichiometry, but it is not evident that such a requirement also applies to the longitudinal constant along [111]. The equality of C_{11} and C_L near 40 m/o Y_2O_3 requires the two shear constants C_{44} and C' to be equal at the same composition. Extrapolation of the linear compositional dependencies of log C_{44} and log C' confirms the shear isotropy expected near 40 m/o Y_2O_3, Fig. 19.

The Cauchy condition [18] for a cubic crystal is

$$C_{12} = C_{44} \tag{13}$$

The deviation from this condition, which is evident in Table 7, is not uncommon in fluorite crystals where the anion sites lack inversion symmetry. In general, the Cauchy condition of the crystals does not change much with either temperature or composition. What little temperature dependence exists, causes C_{12} to approach C_{44} so that there is a minor reduction of some central force interactions with increasing temperature.

Thermal expansion affects the values of the elastic constants. Correction of the constants for thermal expansion was made for cubic crystals using the relation

$$C(T) = C(1-\alpha T), \tag{14}$$

Table 7. Variation of Cauchy relation with temperature for YSZ crystals

Y_2O_3	Cauchy relation (C_{12}-C_{44}), GPa							
m/o	20°C	100°C	200°C	300°C	400°C	500°C	600°C	700°C
11.1	42.5	42.8	43.4	44.0	43.1	39.2	39.1	39.1
12.1	43.5	43.9	44.9	45.1	44.2	38.9	33.9	31.3
15.5	42.8	43.3	43.9	44.5	45.2	44.6	43.2	44.0
17.9	41.7	41.9	42.3	42.5	42.3	39.5	39.5	38.1

where α is the linear coefficient of thermal expansion. An average expansion coefficient for the crystals was taken from available data [46-48] and assumed to be composition independent in the temperature range 20-700°C with uncertainty of $\pm(10^{-9})T/°C$. The coefficient is expressed as

$$\alpha(T) = (8+0.003T)10^{-6}/°C \qquad (15)$$

The elastic constants corrected for thermal expansion are given, together with those uncorrected, for different YSZ crystals in Tables 9, 10, 11, and 12 in the Appendix.

Internal consistency was checked for all crystals by comparing C_{11} values measured directly from mode 4 (see Table 1) with those obtained from a combination of data from modes 1, 2, and 3 in the form

$$C_{11} = \frac{1}{2}(C_{11}+C_{12}+2C_{44}) + \frac{1}{2}(C_{11}-C_{12}) - C_{44} \qquad (16)$$

Agreement to better than 0.5% was found at all temperatures. Table 8 shows the results at room temperature and some additional measurements.

Prediction of polycrystalline elastic behavior can be made from the single-crystalline elastic constants using the Voigt-Reuss-Hill averaging procedures [49]. Young's, bulk and shear moduli and Poisson's ratio were calculated and the results are given at different temperatures in steps of

Table 8. Internal consistency of redundant evaluation at room temperature

Constant	Method of Evaluation	Constant (GPa) of different m/o Y_2O_3 crystals			
		11.1	12.1	15.5	17.9
C_L	(a) Directly from mode 1	313.0	316.4	319.5	319.3
	(b) Directly from mode 5	312.8	316.5	318.9	319.3
C'	(a) Directly from mode 2	150.4	149.5	144.5	138.9
	(b) Directly from mode 6	150.4	149.5	144.1	139.1
C_{44}	(a) Directly from mode 3	60.0	61.6	65.9	69.1
	(b) Directly from mode 7	59.9	61.9	65.9	69.3
	(c) From modes (1+2-4)	60.5	62.0	66.0	69.0
C_{11}	(a) Directly from mode 4	403.2	404.9	397.9	389.2
	(b) From modes (1+2-3)	403.4	405.1	398.1	389.2

100°C in Tables 13, 14, 15, and 16 in the Appendix for the respective polycrystalline aggregates of YSZ of 11.1, 12.1, 15.5, and 17.9 m/o Y_2O_3.

Room temperature values of Young's, bulk and shear moduli are plotted against composition as Y/Zr atom ratio in Fig. 20. All three moduli show a general increase with yttria content except the bulk modulus, which decreases above 12.1 m/o Y_2O_3. The values of the three moduli and the degree of their compositional dependencies decrease in a decreasing order of Young's, bulk and shear moduli. Each of the compositional behaviors of these moduli is viewed as an average effect of the compositional dependencies of the single-crystalline elastic constants involved in each modulus.

Elasticity data for polycrystalline YSZ are sparse. The only published data are those of Buckley and Braski [50] who indicated that Young's modulus of YSZ containing 3.5-8.8 m/o Y_2O_3 decreases with increasing temperature but increases with Y_2O_3 concentration. Our data are in qualitative agreement, showing a higher value of the elastic modulus of the 8.1 m/o Y_2O_3 alloy (223 GPa) at room temperature compared to Buckley's modulus of 8.8 m/o Y_2O_3 specimen (165 GPa).

Comparison was also made with yttria-stabilized hafnia (YSH) at different temperatures. ZrO_2 and HfO_2 are very

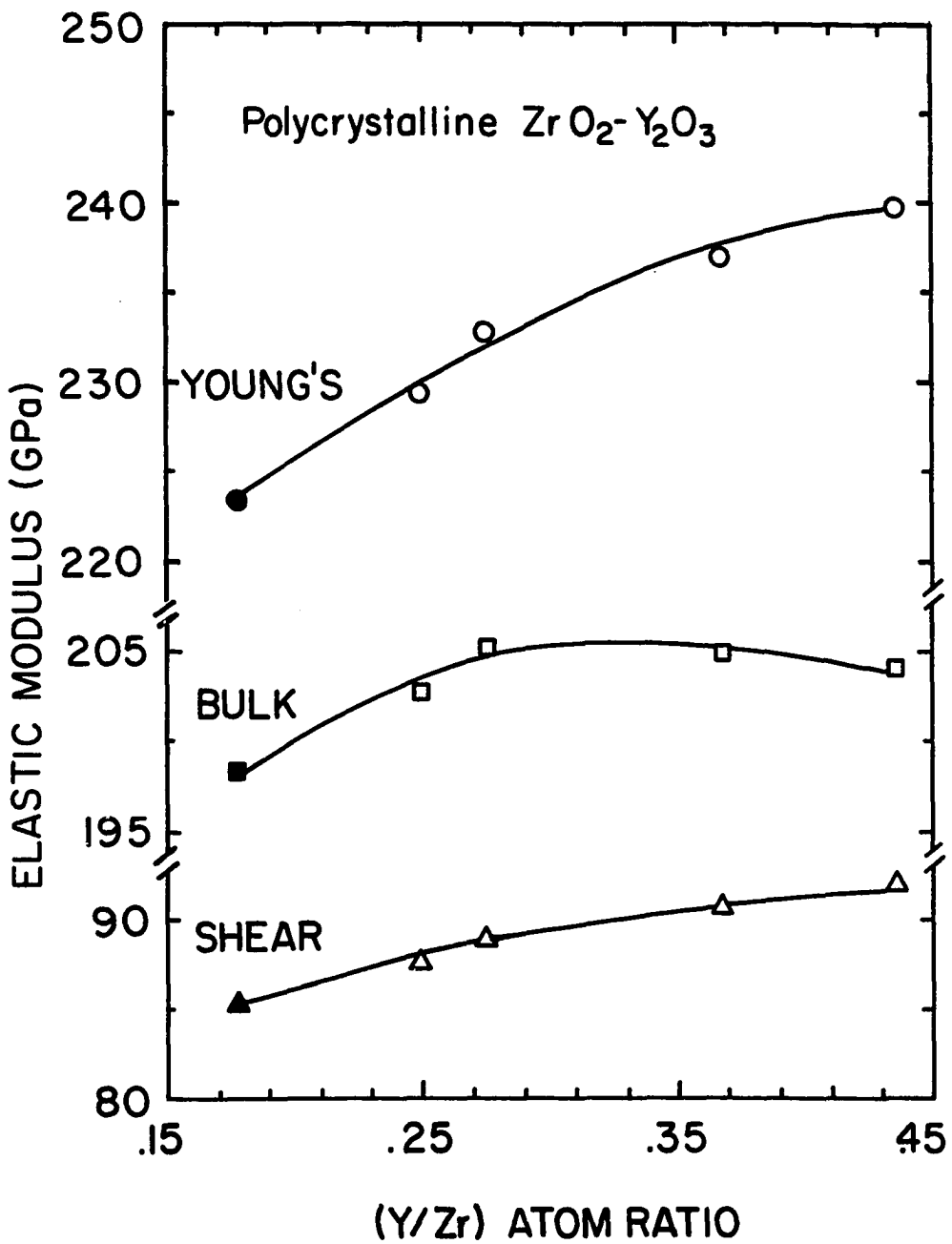

Figure 20. Variations of polycrystalline moduli with composition of YSZ crystals at different temperatures. The 8.1 m/o Y_2O_3 values are shown in solid symbols for the same reason as before

similar oxides characterized by high melting temperatures, high chemical stability, and the same yttria-stabilized structure [51]. Fig. 21 shows a comparison of the temperature dependence of the relative Young's modulus of 17.9b m/o YSZ with that of 20 m/o YSH measured by Dole et al. [52] with a sonic resonance technique. The relative modulus ws chosen because it indicates the relative loss in strength with temperature. The relative modulus is defined at a specific temperature as the ratio of the modulus at that temperature to the modulus at room temperature. In comparison with YSH, the present YSZ shows higher values of the elastic modulus at all temperatures with better retention of strength.

Above room temperature, the elastic moduli of YSZ decrease almost linearly with increasing temperature, which is indicative of good high temperature refractory oxides. Poisson's ratio of YSZ is almost constant (0.30-0.32) at all temperatures and compositions.

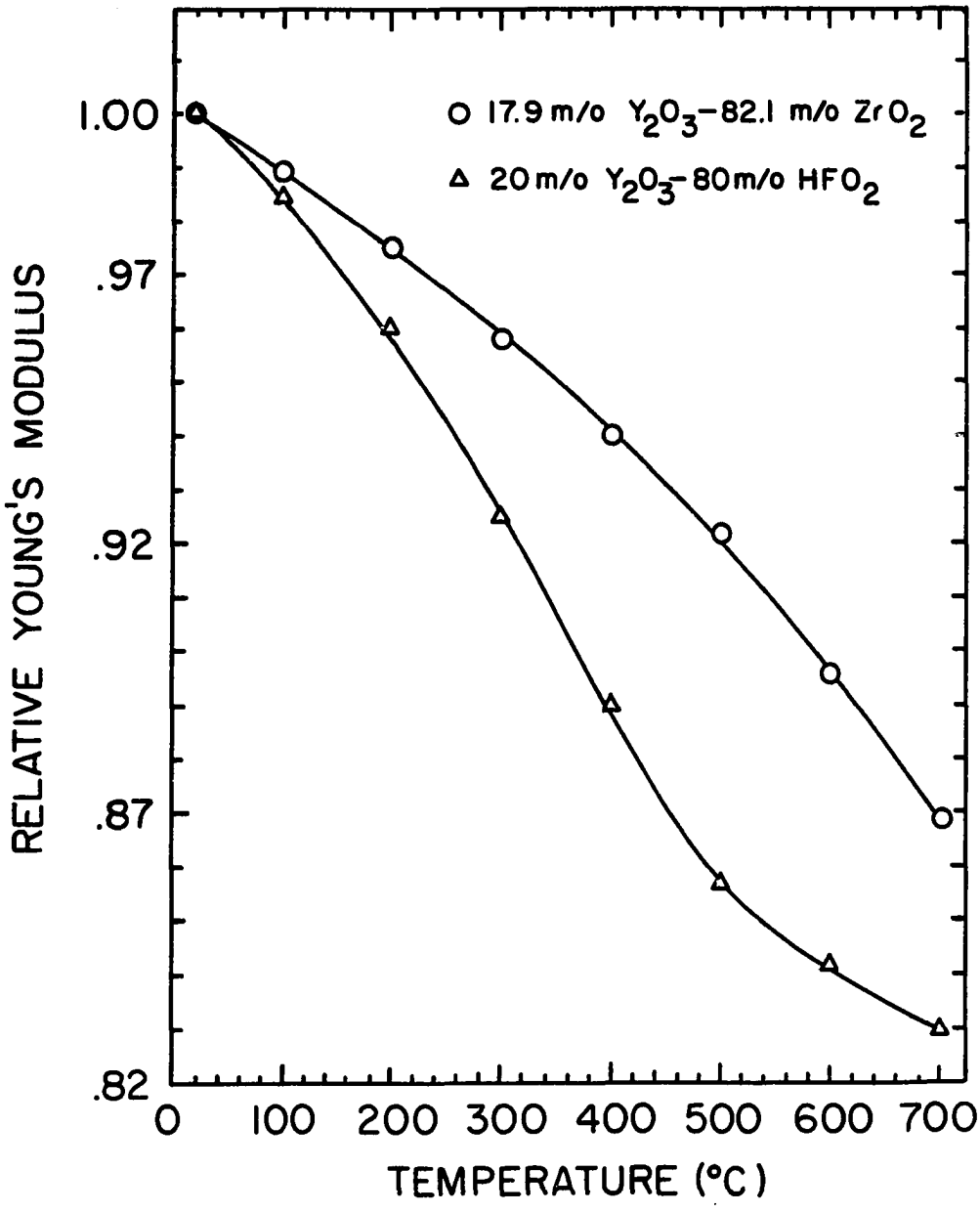

Figure 21. Comparison of the temperature dependence of the relative Young's modulus of the 17.9 m/o YSZ and 20 m/o YSH. The relative modulus is defined as the ratio of the modulus at a specific temperature to the modulus at room temperature

4. SUMMARY

The three independent elastic constants of the cubic YSZ crystals show highest values for C_{11}, intermediate for C_{12}, and smallest values for C_{44} at all temperatures and compositions studied in the present investigation.

The compositional dependencies of the independent constants at room temperature show a decrease in C_{11} but increase in both C_{12} and C_{44} upon increasing Y_2O_3 content. This behavior is explained in terms of the interactomic force interactions between ions. The most important contributions to elastic constants are the Coulomb forces and the Born-Mayer repulsive overlap forces of the first nearest neighbors. The slope of the compositional dependence curves of the constants is primarily determined by the Coulombic contribution, which is a much stronger function of composition than the contribution from the short-range repulsive forces.

The high Debye temperatures of the YSZ crystals are characteristic of the strong interatomic interactions. Debye temperatures were noted to increase with increasing Y_2O_3 concentration, and a linear relationship exists between these characteristic temperatures and the square root of the inverse masses per formula. This observation is consistent

with lattice dynamics principles. Debye temperature is proportional to a characteristic cut-off frequency at sufficiently low temperature. In a harmonic approximation and with neglect of any change in force constants, the cut-off frequency should be inversely proportional to the square root of the vibrating masses.

The temperature dependencies of the elastic constants show a regular decrease with increasing temperature due to the combined effects of thermal expansion and anharmonicity. An exception was observed for the 8.1 m/o Y_2O_3 crystal which shows a nonreproducible anomalous temperature dependence. This observation is not understood.

Shear anisotropy in YSZ is pronounced and it decreases linearly with increasing Y_2O_3 content but increases with temperature. Longitudinal and shear constants along different crystallographic directions indicate, upon extrapolation, elastic isotropy of YSZ crystals at a composition near 40 m/o Y_2O_3 where a number of investigations have established the presence of an ordered phase ($Zr_3Y_4O_{12}$) with a rhombohedral symmetry.

Polycrystalline moduli (Young's, bulk and shear) of YSZ calculated from single-crystalline elastic constants, show a general increase with increasing Y_2O_3 content, except for the bulk modulus which decreases above 12.1 m/o Y_2O_3. The

temperature dependencies of each modulus is almost linear, which is indicative of good high temperature refractory oxides. Poisson's ratio of the crystals is almost independent of both temperature and composition.

5. BIBLIOGRAPHY

1. Weppner, W. Z. Naturforsch. 1976, 31a, 1336.

2. Subbarao, E. C. In "Advances in Ceramics"; Heuer, A. H.; Hobbs, L. W., Eds.; The American Ceramic Society: Ohio, 1981; Vol. 3, Chapter 1.

3. McCullough, J. D.; Trueblood, K. N. Acta Cryst. 1959, 12, 507.

4. Anderson, R. C. In "High Temperature Oxides"; Alper, A. M., Ed.; Academic Press: New York, 1970; Part II, Chapter 1.

5. Chistyi, I. L.; Fabelinskii, I. L.; Kitaeva, V. F.; Osiko, V. V.; Pisarevskii, Yu. V.; Sil'vestrova, I. M.; Sobolev, N. N. J. Raman Spectrosc. 1977, 6, 183.

6. Wagner, C. Naturwissenschaften 1943, 31, 265.

7. Hund, F. Z. Elektrochem. 1951, 55, 363.

8. Morinaga, M.; Cohen, J. B.; Faber, Jr., J. Acta Cryst. 1979, A35, 789.

9. Morinaga, M.; Cohen, J. B.; Faber, Jr, J. Acta Cryst. 1980. A36, 520.

10. Aleshin, E.; Roy, R. J. Am. Ceram. Soc. 1962, 45, 18.

11. Scott, H. G. J. Mater. Sci. 1975, 10, 1527.

12. Pascual, C.; Duran, P. J. Am. Ceram. Soc. 1983, 66, 23.

13. Duwez, P.; Brown, Jr., F. H.; Odell, F. J. Electrochem Soc. 1951, 98, 56.

14. Stubican, V. S.; Hink, R. C.; Ray, S. P. J. Am. Ceram. Soc. 1978, 61, 17.

15. Fu-kang, F.; Kuznetsov, A. K.; Keler, E. K. Izv. Akad. Nauk SSR, Otd. Khim. Nauk 1963, 7, 601.

16. Ray, S. P.; Stubican, V. S.; Cox, D. E. Mat. Res. Bull. 1980, 15, 1419.

17. Scott, H. G. J. Mater. Sci. 1977, 12, 311.

18. Kittel, C. "Introduction to Solid State Physics"; John Wiley: New York, 1953; Chapter 3.

19. Aleksandrov, V. I.; Kitaeva, V. F.; Kozlov, I. V.; Osiko, V. V.; Sobolev, N. N.; Tatarintsev, V. M.; Chistyi, I. L. Sov. Phys. Crystallogr. 1974, 18, 682.

20. Aleksandrov, V. I.; Kitaeva, V. F. ; Osiko, V. V.; Sobolev, N. N.; Tatarintsev, V. M.; Chistyi, I. L. Sov. Phys-Lebedev Inst. Reports 1975, 3, 23.

21. Aleksandrov, V. I.; Kitaeva, V. F.; Kozlov, I. V.; Osiko, V. V.; Sobolev, N. N.; Tatarintsev, V. M.; Chistyi, I. L. Sov. Phys. Solid State 1975, 16, 1456.

22. Pace, N. G.; Saunders, G. A.; Sumengen, Z.; Throp, J. S. J. Mater. Sci. 1969, 4, 1106.

23. Farely, J. M.; Throp, J. S.; Ross, J. S.; Saunders, G. A. J. Mater. Sci. 1972, 7, 475.

24. Aleksandrov, V. I.; Osiko, V. V.; Prokhorov, A. M.; Tatarintsev, V. M. In "Current Topics in Materials Science"; Kaldis, E., Ed.; North Holland: New York, 1978; Vol. 1, Chapter 6.

25. Greiner, J. D.; Bailey, D. M. Rev. Sci. Instrum. 1974, 45, 1032.

26. Pribil, R.; Horacek, J. Chemist-Analyst 1967, 56, 76.

27. May, J. E. IRE Natl. Conv. Rec. 1958, 6, 134.

28. Papadakis, E. P. J. Acoust. Soc. Am. 1967, 42, 1045.

29. Chung, D. H.; Silversmith, D. J.; Chick, B. B. Rev. Sci. Instrum. 1969, 40, 718.

30. McSkimin, H. G. J. Acoust. Soc. Am. 1961, 33, 606.

31. Papadakis, E. P. J. Acoust. Soc. Am. 1968, 44, 724.

32. McSkimin, H. J. IRE Trans. PGUE 1957, 5, 25.

33. "Eutectic Data". U.S. Government Report, ERDA, No. TID-27163-P1/76.

34. Cochran, W. Crit. Rev. Sol. St. Sci. 1971, 2, 1.

35. Axe, J. D. Phys. Rev. 1965, 139A, 1215.

36. Srinivasan, R. Phys. Rev. 1968, 165, 1041.

37. Srinivasan, R. Phys. Rev. 1968, 165 1054.

38. Fuchs, K. Proc. Roy. Soc. 1936, 153A, 622.

39. Pauling, L. Z. Kristallog. 1928, 67, 377.

40. Overton, Jr., W. C.; Schuch, A. F. Los Alamos, New Mexico, Dec. 1966, LA-3615-MS, UC-34, Physics, TID-4500.

41. Kittel, C. "Thermal Physics"; John Wiley: New York, 1969; Chapter 16.

42. Schannette, G. W.; Smith, J. F. J. Appl. Phys. 1969, 40, 79.

43. Newnham, R. E. "Structure-Property Relations"; Springer-Verlag: New York, 1975; Chapter 6.

44. Sawyer, J. O.; Hyde, B. G.; Eyring, L. Bull. Soc. Chem. Fr. 1965, 4, 1190.

45. Love, A. E. H. "A Treatise on the Mathematical Theory of Elasticity"; Dover: New York, 1944; Chapter 6.

46. Mazdiyasni, K. W.; Lynch, C. T.; Smith, II, J. S. J. Am. Ceram. Soc. 1967, 50, 532.

47. Glushkova, V. B.; Osiko, V. V.; Shcherbakova, L. G.; Aleksandrov, V. I.; Paputskii, Yu. N.; Tatarintsev, V. M. Inorg. Mater. (USSR) 1978, May, 1751.

48. Nielsen, T. H.; Leipold, M. H. J. Am. Ceram. Soc. 1964, 47, 155.

49. Hill, R. Proc. Phys. Soc. London 1952, 65A, 349.

50. Buckley, J. D.; Braski, D. N. J. Am. Ceram. Soc. 1967, 50, 220.

51. Ruh, R.; Garrett, H. J.; Domagala, R. F.; Tallan, N. M. J. Am. Ceram. Soc. 1968, 51, 23.

52. Dole, S. L.; Hunter, Jr., O.; Calderwood, F. W. J. Am. Ceram. Soc. 1980, 63, 136.

6. APPENDIX

Table 9. Variation of single-crystal elastic constants with temperature of 11.1 m/o YSZ before and after thermal expansion correction

	Elastic constant (GPa)									
	Uncorrected					Corrected				
T (°C)	C_{11}	C_{12}	C_{44}	C_L	C'	C_{11}	C_{12}	C_{44}	C_L	C'
20	403.5	102.4	59.9	313.0	150.7	403.4	102.3	59.9	313.0	150.7
100	400.5	101.9	59.1	310.2	149.3	400.2	101.8	59.0	310.0	149.2
200	396.2	101.2	57.8	306.2	147.3	395.6	101.0	57.7	305.7	147.0
300	390.8	100.1	56.1	301.1	144.9	389.8	99.8	56.0	300.3	144.5
400	383.4	97.4	54.3	293.6	141.8	382.0	97.1	54.1	292.5	141.3
500	374.9	91.6	52.4	285.7	141.6	373.1	91.2	52.2	284.3	140.9
600	366.8	89.5	50.4	278.5	138.7	364.7	88.9	50.1	276.9	137.9
700	359.1	87.4	48.3	271.6	135.8	356.6	86.8	48.0	269.7	134.9

Table 10. Variation of single-crystal elastic constants with temperature of 12.1 m/o YSZ before and after thermal expansion correction

T (°C)	Elastic constant (GPa)									
	Uncorrected					Corrected				
	C_{11}	C_{12}	C_{44}	C_L	C'	C_{11}	C_{12}	C_{44}	C_L	C'
20	405.1	105.3	61.8	316.5	149.4	405.1	105.2	61.8	316.4	149.4
100	401.9	104.9	61.0	314.1	148.2	401.6	104.8	60.9	313.9	148.1
200	397.3	104.5	59.6	305.9	146.6	396.6	104.3	59.5	310.1	146.3
300	392.3	103.2	58.1	305.9	144.6	391.2	102.9	57.9	305.1	144.3
400	386.5	100.8	56.6	299.7	142.3	385.1	100.4	56.4	298.6	141.8
500	380.7	93.9	55.0	292.3	143.4	378.9	93.4	54.8	290.9	142.7
600	374.3	87.4	53.5	284.3	143.4	372.1	86.9	53.2	282.6	142.6
700	367.4	83.2	51.9	277.2	142.1	364.8	82.6	51.5	275.2	141.1

Table 11. Variation of single-crystal elastic constants with temperature of 15.5 m/o YSZ before and after thermal expansion correction

	Elastic constant (GPa)									
	Uncorrected					Corrected				
T (°C)	C_{11}	C_{12}	C_{44}	C_L	C'	C_{11}	C_{12}	C_{44}	C_L	C'
20	397.6	108.6	65.8	318.6	144.1	397.5	108.6	65.8	318.5	144.1
100	394.9	108.3	65.0	316.3	143.0	394.5	108.2	64.9	316.1	142.9
200	390.4	107.5	63.6	312.6	141.5	389.8	107.3	63.5	312.1	141.2
300	385.8	106.6	62.1	308.4	139.7	384.7	106.4	61.9	307.6	139.4
400	380.9	105.3	60.1	303.3	137.8	379.5	105.0	59.9	302.2	137.3
500	375.4	102.6	58.0	297.0	136.4	373.6	102.1	57.7	295.6	135.7
600	369.0	98.8	55.6	289.5	135.1	366.8	98.2	55.3	287.8	134.3
700	362.8	97.0	53.0	282.9	132.9	360.2	96.3	52.6	280.9	132.0

Table 12. Variation of single-crystal elastic constants with temperature of 17.9 m/o YSZ before and after thermal expansion correction

	Elastic constant (GPa)									
	Uncorrected					Corrected				
T (°C)	C_{11}	C_{12}	C_{44}	C_L	C'	C_{11}	C_{12}	C_{44}	C_L	C'
20	390.4	110.8	69.1	319.2	139.4	390.4	110.7	69.0	319.1	139.4
100	387.4	110.0	68.1	316.5	138.4	387.0	109.9	68.1	316.3	138.2
200	383.5	109.1	66.8	312.8	136.8	382.8	108.9	66.7	312.2	136.6
300	379.1	107.8	65.3	308.2	135.1	378.1	107.5	65.2	307.4	134.8
400	374.7	105.9	63.6	302.8	133.4	373.4	105.6	63.3	301.7	132.9
500	370.0	101.0	61.5	297.0	134.5	368.2	100.5	61.2	295.6	133.8
600	363.5	98.6	59.1	290.2	132.4	361.4	98.1	58.8	288.5	131.7
700	356.3	94.7	56.6	282.0	130.8	353.8	94.0	56.2	280.0	129.9

Table 13. Polycrystalline elastic moduli of 11.1 m/o YSZ at different temperatures

T (°C)	Modulus (GPa)			Poisson's Ratio
	Young's	Bulk	Shear	
20	229.4	202.7	87.6	.31
100	226.8	201.4	86.5	.31
200	223.1	199.5	85.0	.31
300	218.3	197.0	83.1	.32
400	212.9	192.8	81.0	.32
500	207.5	186.1	79.1	.31
600	201.4	181.9	76.7	.32
700	195.2	178.0	74.2	.32

Table 14. Polycrystalline elastic moduli of 12.1 m/o YSZ at different temperatures

T (°C)	Modulus (GPa)			Poisson's Ratio
	Young's	Bulk	Shear	
20	232.8	205.2	88.9	.31
100	230.3	203.9	87.9	.31
200	226.3	202.1	86.2	.31
300	221.9	199.5	84.5	.31
400	217.7	196.0	82.9	.31
500	214.1	189.5	81.7	.31
600	210.2	183.0	80.4	.31
700	205.6	177.9	78.8	.31

Table 15. Polycrystalline elastic moduli of 15.5 m/o YSZ at different temperatures

T (°C)	Modulus (GPa)			Poisson's Ratio
	Young's	Bulk	Shear	
20	237.0	204.9	90.7	.31
100	234.5	203.8	89.7	.31
200	230.8	201.8	88.2	.31
300	226.4	199.7	86.4	.31
400	221.5	197.2	84.4	.31
500	216.2	193.5	82.3	.31
600	210.2	188.9	80.1	.31
700	203.6	185.6	77.4	.32

Table 16. Polycrystalline elastic moduli of 17.9 m/o YSZ at different temperatures

T (°C)	Modulus (GPa)			Poisson's Ratio
	Young's	Bulk	Shear	
20	239.8	204.0	92.0	.30
100	237.2	202.5	90.9	.30
200	233.7	200.6	89.5	.31
300	229.8	198.2	88.0	.31
400	225.4	195.5	86.2	.31
500	221.0	190.7	84.6	.31
600	214.9	186.9	82.2	.31
700	208.5	181.9	79.7	.31

7. ACKNOWLEDGEMENTS

I would first like to acknowledge my wife, Hanaa, who has shown both support and patience throughout my work.

I owe special thanks to Dr. J. F. Smith, my major professor, for his knowledgeable guidance and critical analysis in the preparation and completion of this dissertation; and to J. D. Greiner for assistance with the experimental work and computer; and Dr. M. F. Berard for helpful discussions and encouragement during this investigation. Thanks are also due to G. W. Jordan and M. D. Rasmussen and to many other staff, students and friends who made this project easier.

Finally, I would like to extend my sincere gratitude to the Egyptian Government for support during the course of this work.